

A HAIR CELL-SPECIFIC VESICULAR GLUTAMATE TRANSPORTER IS
REQUIRED FOR AUDITORY AND VESTIBULAR FUNCTION IN ZEBRAFISH

by

Sean N. Wolfson

A THESIS

Presented to the Department of Cell and Developmental Biology

and the Oregon Health & Science University

School of Medicine

in partial fulfillment of

the requirements for the degree of


Master of Science


2007

School of Medicine
Oregon Health & Science University

CERTIFICATE OF APPROVAL

This is to certify that the Master's thesis of
Sean N. Wolfson
has been approved


Teresa Nicolson, Ph.D.


Peter G. Gillespie, Ph.D.



Wenbiao Chen, Ph.D.

TABLE OF CONTENTS

Acknowledgements.....	iii
Abstract.....	iv
1. Introduction.....	1
1.1 Hair Cell Structure and Function.....	2
1.1.1 The Hair Bundle.....	2
1.1.2 The Hair Cell Afferent Synapse.....	5
1.2 Auditory and Vestibular Organs in Zebrafish....	9
1.3 Vesicular Glutamate Transporters.....	10
2. Materials and Methods.....	13
3. Results.....	23
3.1 The <i>asteroid</i> Phenotype.....	23
3.2 Mapping.....	23
3.3 Sequencing.....	24
3.4 <i>In situ</i> Hybridization.....	25
3.5 Phenocopy.....	26
3.6 Rescue.....	27
3.7 Immunohistochemistry.....	28
3.8 Ultrastructure and Morphometry.....	29
Figures.....	31-37

4. Discussion.....	38
4.1 Mis-splicing of <i>vglut3</i> mRNA.....	38
4.2 <i>vglut3</i> Distribution.....	40
4.3 Phenocopy.....	42
4.4 No Compensatory Increase in Ribbon Number or Size..	44
4.5 Synaptic Vesicles at the Hair Cell Ribbon Synapse.....	44
4.5.1 SV Recruitment.....	45
4.5.2 SV Biogenesis and Recycling.....	46
4.6 Future Directions.....	48
5. Summary.....	50
6. References.....	51
Appendix I.....	63
Appendix II.....	64

ACKNOWLEDGEMENTS

First and foremost, I would like to thank Teresa Nicolson for her mentorship and support during my time in her lab. She was ever willing and ready to discuss my project, or the life of a scientist in general, or just about anything, really, and because of her wisdom and warmth I count her as a friend.

I would also like to thank the members of the Nicolson Lab, past and present. For technical assistance, I thank Sarah Song and Felipe Ramos, and for helping keep the Nicolson Lab in working order I thank our lab manager, Sireesha Govada. Our fishroom would have fallen apart without the efforts of Julie Zeppieri. I also thank Zev Einhorn, Greta Glover, Qianyong Liu, Weike Mo, Lavinia Sheets, and Joe Trapani for their helpful discussions and making the Nicolson Lab such a fun place to work. I would also like to thank Jackie DeGagne in the Oregon Hearing Research Center EM Facility.

I thank Robert Duncan for technical assistance with the morpholino experiments reported in this thesis. Much of this data was collected in the weeks immediately preceding the deadline for this thesis, and this could not have happened without Rob's help.

I am particularly indebted to Nikolaus Obholzer, not only for his contribution to the data presented here, but also for countless scientific discussions that informed the direction of this work and interpretation of these results. There are few things I'll miss more about grad school than his camaraderie.

I would also like to thank Sunjong Kwon for his friendship and for teaching me a great many molecular biology and protein biochemistry techniques. In another world, we might have done some great work on mRNA localization. Maybe next time.

I have been affiliated with two graduate programs and three departments in my time at OHSU, and I have received administrative support from many quarters. From the Neuroscience Graduate Program, Liz Lawson-Weber; from the Department of Cell and Developmental Biology, Elaine Offield, Pam Waggoner and Nikki Larson; from the Vollum Institute, Fay Keeling and Leslie Williams; from the Oregon Hearing Research Center, Jill Lilly and Theresa Nims. To all of you, thanks for keeping me on track.

For advice and counseling along the way, I would like to thank Peter Gillespie and Edwin McCleskey.

I thank my Thesis Advisory Committee for their guidance and support.

Finally, I would like to thank my family and friends, for all the usual reasons.

My work in the Nicolson Lab was supported by NIH Training Grant T32 DC005945.

ABSTRACT

Hair cells (HCs) are the sense receptors for the auditory and vestibular systems. I report here that *asteroid*, a gene identified in an ENU mutagenesis screen for deafness/vestibular dysfunction mutants, encodes vesicular glutamate transporter 3 (Vglut3). Hair cells in *ast*^{-/-} fish show normal FM 1-43 uptake—indicative of normal mechanotransduction—and display no obvious morphological defects, suggesting that the *ast* defect is in neurotransmission. *In situ* hybridization shows that *vglut3* is expressed in hair cells of the ear, whereas *vglut1* and *-2* are not. A splicing defect that results in the exclusion of exon 2 from *vglut3* mRNA correlates with the *ast* phenotype; however, the genomic lesion is not located in exonic sequence, suggesting that the lesion is likely in an intronic splicing regulatory element. Morpholinos directed against the *vglut3* start codon and intron 2 splice sites delete exon 2 in ~50% of *vglut3* transcripts and cause a balance defect reminiscent of, though weaker than, the *asteroid* phenotype. While there is no apparent difference in synaptic ribbon number or ribbon localization in *ast* mutants, ultrastructural analysis reveals a decrease in the number of ribbon-associated synaptic vesicles, perhaps indicating a role for Vglut3 in synaptic vesicle biogenesis and/or trafficking. Thus Vglut3 may have roles beyond neurotransmitter transport. These results provide the first unambiguous identification of the hair cell vesicular glutamate transporter, and establish the *asteroid* mutation as a platform on which to conduct further investigation into hair cell synaptic biology.

1. INTRODUCTION

Hair cells are the sensory receptors for the auditory and vestibular systems. Their complex morphology enables them to transduce mechanical stimuli into graded receptor potentials, which cause glutamate release (Glowatzki and Fuchs, 2002) and drive action potentials in primary afferent neurons. The structures of the hair cells and the sensory organs into which they are integrated allow render them exquisitely sensitive to incoming stimuli, and allow information encoding across a very wide dynamic range.

Hair cell ultrastructure has been described in great detail (Tilney et al., 1983; Tilney and Saunders, 1983; Tilney and DeRosier, 1986), as have the mechano-electrical properties of the apical stereocilia which give hair cells their name (Vollrath et al., 2007) and the electrical properties of the hair cell afferent synapse (Moser et al., 2006); however, the identification of specific proteins required for hair cell function and their placement in mechanistic models has lagged behind that of other sensory systems. This is in part due to the relative scarcity of starting material in any particular organism: one mouse inner ear, for example, contains only about 10,000 hair cells, while one eye contains tens of millions of photoreceptors. While some progress has been made {Shin, 2007 #1}, these numbers suggest the difficulty of biochemical approaches to isolating proteins required for morphogenesis, mechanotransduction or synaptic transmission in hair cells.

Genetic approaches have fared better. A number of deafness genes have been cloned from mice and humans, in particular the suite of genes underlying Usher syndrome (Kremer et al., 2006). More recently, an ENU mutagenesis screen in the

zebrafish *Danio rerio* has recovered a number of complementation groups whose mutated loci are required for auditory and vestibular function (Nicolson et al., 1998).

The phenotypes of these so-called circler mutants are found in all stages of the sensory transduction process. Mechanotransduction is defective in *cadherin 23* (*cdh23*) mutants (Sollner et al., 2004), while lesions in *protocadherin 15* (*pcdh15*) result in a splayed bundle phenotype (Seiler et al., 2005). Synaptic vesicle recycling is impaired in *comet* mutants, though the corresponding gene has not yet been identified, and transmission is eliminated in fish with mutations in the calcium-channel gene *cav1.3* (Sidi et al., 2004). The main subject of this thesis is the *asteroid* circler mutant, a putative transmission-defective line which carries a mutation in the *D. rerio* orthologue of vesicular glutamate transporter 3 (Vglut3).

1.1. Hair Cell Structure and Function

There are two primary functional domains in hair cells: the apical hair bundle, where mechanotransduction occurs, and the basal ribbon synapse, which is the site of neurotransmission. Each relies on a highly specialized morphology to accomplish its task. While the work presented below focuses primarily on molecules involved in transmission, a brief introduction of mechanotransduction is in order.

1.1.1 The Hair Bundle

The hair bundle is comprised of an array of stereocilia—a misnomer, since they contain no microtubules—and a single kinocilium that is eliminated in mature hair cells of mammals but persists in those of zebrafish. Sterocilia are arranged in rows of increasing height, with the tallest ones residing closest to the kinocilium. When the hair

bundle is deflected toward its kinocilium, mechanosensitive ion channels at the tips open, and the hair cells depolarize.

Stereocilia have an elaborate cytoskeleton. A tightly-packed hexagonal array of actin filaments traverse almost the entire length, dropping off only at the base, where the few bundles that do remain insert into the cuticular plate just under the apical membrane (Tilney et al., 1983). This array is densely populated by the actin-bundling proteins fimbrin and espin, with the result that the stereocilium is a rigid structure that pivots at the base. Despite this tight bundling, actin in stereocilia undergoes rapid turnover (Schneider et al., 2002; Rzadzinska et al., 2004), as do stereociliary plasma membrane (PM) proteins (Grati et al., 2006). Thus, the stereocilium is a dynamic structure.

There are three classes of extracellular linkages between stereocilia. Ankle links are present only between immature stereocilia, and are likely comprised of VLGR1 (McGee et al., 2006) and usherin (Adato et al., 2005), and possibly other proteins. Abundant lateral links, found along the middle 2/3 of the stereocilia, presumably play a role in maintaining hair bundle cohesion, as they are seen linking stereocilia both within and between rows. Lateral links may contain Cdh23 (Michel et al., 2005) and Pcdh15 (El-Amraoui and Petit, 2005), among others, but at present, evidence for this is scant.

The tip link connects each stereocilium to its neighbor in the next (taller) row. It is the tip links that have drawn the most interest because of their direct role in gating the ion channels that mediate mechanotransduction. The evidence implicating tip links in the mechanism of mechanotransduction are: (1) mutations in Cdh23 eliminate both tip links and the mechanotransduction (MET) current (Siemens et al., 2004; Sollner et al., 2004); (2) treatment of hair cells with calcium chelators, lanthanum, or elastase both degrades

tip links and eliminates the MET current (Preyer et al., 1995; but see Meyer et al., 1998); and (3) following washout of Ca^{2+} -chelators, tip links and mechanotransduction recover with similar timecourses (Zhao et al., 1996).

The tip link complex includes Cdh23 and probably Pcdh15 (Ahmed et al., 2006). Since at least Cdh23 can form *trans* homotypic interactions in cell culture (Siemens et al., 2004), it is presumed that it does so in tip links as well. The tip link complex is also anchored to the cytoskeleton through interactions with one or more members of the Usher family of stereociliary proteins (El-Amraoui and Petit, 2005), and to the mechanoelectrical transduction (MET) channel as well (Vollrath et al., 2007).

A comprehensive review of the process of hair cell mechanotransduction is beyond the scope of this thesis (see Vollrath et al., 2007 instead), but the basic mechanism is as follows: When a hair bundle is deflected along its axis of excitation, the rigid stereocilia pivot at the base. Because each row of the hair bundle contains stereocilia of successively greater heights, this pivoting causes the tips of adjacent stereocilia to shear away from each other. As the distance between the tips of the stereocilia grows, tension is exerted on the tip link. This force is transduced directly to the mechanotransduction apparatus and the hair cell depolarizes. When the stimulus ends, tension in the transduction apparatus returns the hair bundle to its resting position, and the cycle can begin again.

1.1.2 The Hair Cell Afferent Synapse

The synaptic specialization of hair cells is the ribbon synapse. Also found in photoreceptors and rod bipolar cells (Prescott and Zenisek, 2005), the ribbon body is thought to facilitate the rapid release and replenishment of synaptic vesicles.

The distinguishing morphological feature of the ribbon synapse is an electron-dense structure apposed to the presynaptic active zone and known as the ribbon body. Ribbon bodies in hair cells tend toward the spherical, while those of photoreceptors and rod bipolar cells are generally planar. Whatever their shape, ribbon bodies are surrounded by a halo of synaptic vesicles that are tethered by short filaments of unknown composition.

The only ribbon-specific protein yet identified is Ribeye {Schmitz, 2000 #316}. This protein consists of a functional N-terminal domain that is thought to mediate oligomerization, and an NAD^+ -binding C-terminus identical to the transcription factor CtBP2. This domain organization has led to a structural model of ribbons as aggregates of Ribeye molecules with their C-termini facing the center of the ribbon and their N-termini exposed to the surrounding cytosol (Schmitz et al., 2000).

Other than Ribeye, the proteins found at ribbon synapses do not differ dramatically from those at conventional synapses. The usual complement of presynaptic active zone components are present, though Bassoon seems to engage in a specific interaction with Ribeye to anchor ribbon bodies to the active zone {tom Dieck, 2005 #299}. One difference worth noting is that ribbon synapses apparently employ L-type voltage-gated Ca^{2+} -channels to trigger endocytosis, rather than N- or P/Q-types (Sidi et al., 2004).

Synaptic vesicles (SVs) at the ribbon synapse also contain the usual complement of proteins, with the exception of synapsins and rabphilins (Von Kriegstein et al., 1999). One group has reported the absence of typical Synaptotagmins from hair cells of the guinea pig (Safieddine and Wenthold, 1999), but another group has put Otoferlin forward as a substitute Ca^{2+} -sensor (Roux et al., 2006).

There are three morphologically distinguishable SV pools at the ribbon synapse. The readily-releaseable pool (RRP) is defined by those vesicles docked at the active zone (i.e. between the ribbon and the presynaptic PM). The recycling pool comprises those SVs tethered to the ribbon but not at the active zone. The reserve pool is found in the cytoplasm, near but not tethered to the ribbon. On the other hand, kinetic measurements of SV exocytosis using whole-cell capacitance measurements resolve just two pools: a fast component representing the RRP, and a slow component that presumably accounts for the recycling and reserve pools. The RRP was found to consist of 280 vesicles, and was released with a time constant of 10 ms, setting the upper limit for the initial rate of release at 28,000 SV/sec (Moser and Beutner, 2000). The remainder of the SVs were released more slowly, at approximately 6000 SV/sec, but even this value is well above that seen at conventional synapses. A subsequent report using optical methods (Griesinger et al., 2005) reported a release rate of approximately 1400 SV/sec; combined with replenishment rate of 1100 SV/sec (Moser and Beutner, 2000), the hair cell has an apparently inexhaustible supply of SVs.

The presumed function of the ribbon body is to recruit SVs from the reserve pool to the recycling pool and facilitate their transport to the RRP, all at extremely high rates (Griesinger et al., 2005). Indeed, sustained depolarization was found to preferentially

deplete SVs tethered to the basal hemisphere of the ribbon body in bullfrog saccular hair cells (Lenzi et al., 2002). How either of these tasks may be accomplished is unknown: the C-terminus of Ribeye, which is hypothesized to interact with SVs, has not been shown to bind to any SV proteins, nor have any SV proteins been identified that specifically mediate recruitment to the ribbon. As for transport from the recycling pool to the RRP, two groups have reported localization of the kinesin motor KIF3A to photoreceptor ribbons {Muresan, 1999 #325; tom Dieck, 2005 #299}, but as ribbons are not known to contain microtubules, a role for KIF3A in SV conveyance remains uncertain.

Whatever the case, it now appears that ribbon bodies are not absolutely required for SV exocytosis in hair cells. Mice lacking Bassoon fail to anchor ribbon bodies at the hair cell active zone (Khimich et al., 2005), yet SVs in these cells can still fuse with the PM, albeit at a reduced rate. The authors conclude that ribbons are required for synchronizing SV fusion to ensure proper temporal coding of auditory stimuli, which is consistent with other findings suggesting that IHCs engage in multivesicular release (Glowatzki and Fuchs, 2002) and that SVs away from hair cell active zones are still able to fuse with the PM in an activity-dependent manner (Edmonds et al., 2004).

As described above, hair cell ribbon synapses are capable of replenishing the RRP at rates of up to 1100 per second. Clathrin-coated invaginations of the PM showing the classic “omega-profile” associated with AP2-dependent endocytosis have been observed near ribbons in hair cells (Lenzi et al., 1999), but it is unlikely that this pathway alone can satisfy this level of demand.

Two alternative mechanisms have been proposed: reuse mechanisms such as “kiss-and-stay” and “kiss-and-run” in which vesicles do not lose their identity upon

fusion with the PM (i.e., no subsequent requirement for sorting SV proteins from PM proteins during endocytosis) and recycle locally; and an endosomal or cisternal recycling model, wherein SVs are resynthesized in bulk from endosomal intermediates by an AP3-dependent process (Sudhof, 2004). Evidence in hair cells for reuse mechanisms is scant, but large cisternae have been observed close to ribbons in hair cells following sustained depolarizations, and may reflect endosomal SV recycling intermediates (Lenzi et al., 2002).

A third model, really a modification of the endosomal recycling model, has been proposed, and involves transcytosis of membrane retrieved from the apical hair cell plasma membrane and trafficked through the Golgi apparatus on its way back to the ribbon synapse (Griesinger et al., 2002; Griesinger et al., 2004; Griesinger et al., 2005). This model was derived from experiments using the styryl dye FM 1-43 to mark endocytic vesicles. FM 1-43 is commonly used to track endocytic vesicles in neurons, but its utility in hair cells is complicated by the findings of many groups that it passes through the MET channel pore (Gale et al., 2001; Meyers et al., 2003). Indeed, in the Nicolson Lab, full FM 1-43 loading of hair cells in the neuromasts of the lateral line organ can be achieved in as little as 30 seconds. The experiments supporting the transcytosis model (Griesinger et al., 2005) were not conducted in the presence of a known impermeant MET channel blocker (Farris et al., 2004), and so it seems premature to ascribe the FM 1-43 signal found at the basal membrane solely to a transcytotic pathway. Nevertheless, it is formally possible that such a mechanism is operant, and that it contributes significantly to SV replenishment.

1.2 Auditory and Vestibular Organs in Zebrafish

The hair cells described above are organized into organs specialized for the detection of sound waves in the environment or accelerations of the head. In vertebrates, these organs are found in the inner ear. Higher vertebrates such as mammals have highly complex inner ears: while a review of their structure and function is beyond the scope of this introduction, suffice it to say that they are exquisitely sensitive, and can detect stimuli across a wide dynamic range and a broad range of frequencies.

The auditory/vestibular physiology of the zebrafish, while similar in many respects to that of higher vertebrates, is far simpler (see Haddon and Lewis, 1996 for review). Zebrafish have no outer and middle ears per se; rather, sound waves in water are transduced through the swim bladder and the Weberian ossicles (a series of four bones analogous to those of the mammalian middle ear) to the posterior macula of the ear. This macula, along with the anterior macula are overlaid by carbonaceous otoliths and are specialized to detect gravity and other linear accelerations. The cristae in the three semicircular canals detect angular accelerations. Two other macular organs, the lagena and the macula neglecta, arise later in development. All hair cells in the ear synapse onto neurons of the statoacoustic ganglion (VIIIth cranial nerve), which projects to the brainstem.

Zebrafish also possess a system of hair-cell based organs that are specialized to detect vibration and current flow, and thus mediate schooling and escape behaviors among others (for review, see Raible, 2000). This so-called lateral line system comprises small, superficial sensory patches known as neuromasts that themselves comprise a

rosette of hair cells surrounded by supporting cells. Neuromast hair cells synapse with neurons of the posterior or anterior lateral line ganglia, which also project to the brainstem. The stereocilia of neuromast hair cells extend above the surface of the skin, but are covered by a gelatinous cupola. They can be loaded with the MET channel-permeant dye FM 1-43 within seconds, and are thus an attractive system in which to probe general hair cell function *in vivo*.

1.3 Vesicular Glutamate Transporters

In spite of its primacy in excitatory neuronal signaling, the identification of the vesicular transporter for glutamate lagged behind that of other neurotransmitters (NTs). In 1994, brain-specific Na⁺-dependent inorganic phosphate transporter (BNPI) was cloned, and was indeed found to mediate Pi uptake (Ni et al., 1994). Other transporters of this type typically reside at the PM, but follow-up studies on BNPI found that it was localized to synaptic vesicles (Bellocchio et al., 1998). In 1999, the *C. elegans* orthologue of BNPI was found to be required for glutamatergic neurotransmission {Lee, 1999 #606}. Finally, in 2000, two groups (Bellocchio et al., 2000; Takamori et al., 2000) simultaneously identified BNPI as the first isoform of the vesicular glutamate transporter (Vglut1). Vglut2 soon followed (Bai et al., 2001; Fremeau et al., 2001; Hayashi et al., 2001; Herzog et al., 2001a; Takamori et al., 2001a). Finally, a third isoform, Vglut3, was discovered (Fremeau et al., 2002; Gras et al., 2002; Schafer et al., 2002; Takamori et al., 2002).

Like other NT transporters, Vgluts depend on a proton gradient to drive transport across the SV membrane. However, in contrast to vesicular monoamine transporters and

the GABA transporter, Vglut1 and -2 rely far more on the electrical ($\Delta\psi$) component of this gradient than the pH component (Takamori et al., 2000; Herzog et al., 2001b), while Vglut3, is dependent on both (Gras et al., 2002).

Vglut1 and -2 are expressed in complementary regions of the mature mammalian CNS (Fremeau et al., 2004a), although Vglut2 is apparently co-expressed with Vglut1 in a subset of developing neurons in the hippocampi of 1-week old mice (Fremeau et al., 2004b). A Vglut1 knockout has been reported: in addition to silencing of hippocampal pyramidal neurons, a significant reduction was seen in the number of SVs within 300 nm of the active zone in excitatory terminals in the hippocampus and cerebellum, and several SV-associated proteins were underexpressed in hippocampal extracts (Fremeau et al., 2004b).

The distribution of Vglut3 is intriguing, in that it is found in glutamatergic neurons as well as certain populations of GABAergic (Fremeau et al., 2001), serotonergic and cholinergic (Gras et al., 2002) neurons, and even in astrocytes and non-neuronal cell in the kidney and liver. As heterologous expression of Vglut1 (Takamori et al., 2000) or Vglut 2 (Takamori et al., 2001b) is sufficient to enable quantal glutamate release in autaptic cultures of GABAergic neurons, it is possible that neurons traditionally assigned to one NT class may also release glutamate *in vivo*.

As mentioned above, hair cells are glutamatergic. While one group has reported Vglut1 expression at hair cell ribbon synapses in mice (Furness and Lawton, 2003), I will present evidence below that identifies Vglut3 as a hair cell-specific vesicular glutamate transporter. Using a combination of molecular and imaging techniques, I show that *asteroid* circler mutants have a frameshift generating mutation in *vglut3* mRNA that leads

to a non-functional Vglut3 protein. Moreover, this mutation leads to a decrease in the number of synaptic vesicles at hair cell ribbon synapses, and points to a role for Vglut3 beyond mere uptake of neurotransmitter.

2. MATERIALS AND METHODS

Husbandry

All *D. rerio* strains are kept on a 14 hr/10 hr light/dark cycle. To obtain clutches of *asteroid* larvae, previously separated IJ001-ID (heterozygous) males and females were placed in a 1L tank with a grating just above the bottom and left overnight. Mating generally begins within 30 minutes of lights on. Embryos were collected by transferring the pair to a holding tank, removing the grating, and pouring the system water with the embryos through a sieve. The retained embryos were washed into a petri dish with E3 embryo medium (5mM NaCl, 0.17 mM KCl, 0.33 mM CaCl₂, 0.33 mM MgSO₄, 10⁻⁵% methylene blue) and transferred to a 30° C incubator, where they were grown up for up to seven days with periodic refreshing of the medium. Except in rare cases, a two-week minimum between matings was observed.

To obtain embryos for microinjection (see below), pairs were set up overnight in a 2L tank with a divider between the male and female. The following morning, the male and female were combined on the upper side of the divider. Embryos were collected within 20 minutes of pairing.

Sorting

Clutches from IJ001 pairings were subject to three tests. On Day 4 or 5, larvae were visually examined, and those that had aberrant posture (i.e. failure to orient their dorsal sides up) were separated from their siblings. These two pools were then assessed for deafness by tapping the sides of their petri dishes to elicit a startle response. Non-

responders were transferred to a third petri dish, and the swim-trajectories of individual larvae were tested by touching their tails with a fine metal probe. Larvae that failed to orient themselves dorsal-up, showed no startle response, and had spiraling swim-trajectories were classified as *asteroid* mutants. All larvae that were malformed, or that met just one or two of the above criteria, were discarded, and those that failed to meet all three criteria were retained as wild-type siblings.

mRNA and Genomic DNA Extraction

Clutches from Tü/AB, WIK and *asteroid* pairs were grown to >120 hpf and, in the case of *asteroid* clutches, sorted on the basis of phenotype. Day 5 larvae were euthanized with MESAB (4 mg/mL ethyl-*m*-aminobenzoate methanesulphonate, 1% Na₂HPO₄, pH 7.0-7.5) and collected into 2 mL Eppendorf tubes.

For poly(A) mRNA extraction, larvae were transferred to lysis buffer (12 ul/larva) from the MicroPoly(A)Purist Kit (Ambion, Austin, TX) and vortexed for ~1 minute. This crude lysate was then triturated through a 27-gauge needle, and mRNA extraction proceeded according to the manufacturer's instructions.

For genomic DNA extraction, larvae were incubated at 50° C in lysis buffer (10 mM Tris, 1 mM EDTA) in an Eppendorf thermomixer at 500 rpm. Protein was pelleted at 13,000 x g at 4° C, and genomic DNA was phenol/chloroform extracted from the supernatant and resuspended in ddH₂O or Tris-EDTA (pH 8.0).

cDNA Cloning and Rapid Amplification of cDNA Ends (RACE)

For *vglut3*-CDS cloning, a fraction of isolated poly(A)-mRNA was used as a template for first-strand cDNA synthesis using either the RT-for-PCR system (BD Biosciences) or the SuperScript III First-Strand Synthesis System (Invitrogen) and an oligo d(T) primer. First-strand cDNA was then used as a template for conventional PCR with the primers VG3_c1F1.1 and VG3_c1R5L (see table below).

For the 3'RACE of *vglut3* cDNA, oligo d(T)-primed first-strand was generated with the SMART-RACE cDNA Amplification Kit (Clontech, Mountain View, CA). The 3'UTR of *vglut3* was then amplified using a high-T_m gene-specific primer (VG3_3RACE_F2) and the Universal Primer Mix (UPM) included in the kit. The original reaction was used as template in a nested-PCR experiment with VG3_c1F4 and the nested UPM, and the resulting product was cloned into pCR-II and sequenced.

Polymerase Chain Reaction (PCR) and Sequencing

Primers for cDNA cloning, subcloning and sequencing were ordered from either Invitrogen (Carlsbad, CA) or Integrated DNA Technologies (Coralville, IA) and dissolved in Tris-EDTA (pH 8.0) to 20 uM. PCR was carried out with a variety of polymerases, most commonly the BD Advantage Taq DNA Polymerase Mix (BD Biosciences, San Jose, CA). PCR amplicons were either sequenced directly from the PCR reaction following ExoSAP-IT (USB, Cleveland, OH) treatment to degrade amplification primers, or were first extracted from TBE-agarose gels with the QIAquick Gel Extraction Kit (QIAGEN, Valencia, CA) and then submitted directly for sequencing. Occasionally, gel-extracted PCR products were TOPO-cloned into either pCR-II or pCR-ZERO BLUNT (Invitrogen), followed by transformation into TOP-10 chemically

competent DH5a E. coli. After plating, colonies were screen for the presence of insert by colony PCR, and positive colonies were inoculated into overnight cultures, miniprep (QIAprep Spin Miniprep Kit, QIAGEN), and submitted for sequencing. All sequencing was performed by Sequencing Core Facilities either at the Vollum Institute or the OHSU Department of Molecular and Medical Immunology.

Primers

vglut3 cDNA Primers

VG3_cIF1.1	AAGGAGAGATGCCACTGGGGG
VG3_cIF1.2	AGTCCAGTGCAGGAGAGGATGCG
VG3_cIR5L	TCATTGATACTGGGTCTGATATTCCCA TTTTCATAATGATTTGATT
VG3_UTR-F	AGGACTGGGCTGATCCGGAGAACA
VG3_3UTR_R1	AAGTCTCTGATGTTACCAAGGGCACATTTATTTGATT
VG3_F2_3RACE	GGGGCTACATCGTCACTCAAATCCCTGGAGGTTTCA

vglut3 genomic primers

VG3_X1I1_F1	TTGTGGTTCGTTTCTGGATGTTCTGCGG
VG3_X1I1_R1	CTCAGCCTCCTGTGTGTATGTTACAGT
VG3_I1X2_F1	GCTGAACTGTAAGGAGAATAATATCACCTTACTCCC
VG3_I1X2_R1	CCGTATACCGTGAAACCGTCAAACCGT
VG3_X2I2_F1	CAGCAGTCAAATGTTGGAGTCCTTGGT
VG3_X2I2_R1	TGGCCACTGCACTCGTGTGGATGTTAAA

Morpholinos

Morpholinos against the *vglut3* start codon and intron 2 splice sites were obtained from GeneTools, LLC (Philomath, OR) as lyophilized solids and resuspended in RNase-free ddH₂O to 2 mM. Injection solutions were made by diluting this stock with ddH₂O and KCl to final concentrations of 1 mM, 500, 250, 100 and 50 uM for MOs, and 2mM for KCl. Phenol red was added to a final volume of 5% as an injection tracer.

Morpholinos	
VG3-ATG	CCAGTGGCATCTCTCCTTCCCTTTC
VG3-ATG-C	CCAcTGcCATCTgTCgTTCCgTTTC
VG3-X2del	GCTGGCTAAACAATGCAAACATTAG
VG3-X2del-C	GCTcGgTAAAgAATcCAAAGATTAG
VG3-X2del2	ATTTATTTCTGGTTTCACCTGCATG
VG3-X2del2-C	ATTTtTTTgTGGTTTgACgTGgATG

In vitro Transcription

To generate digoxigenin-labeled probes for *in situ* hybridization, the *vglut3* 3' RACE product described above was used as a template for amplification of a ~800 bp fragment comprising the last 250 bp of the CDS and the full-length, 542 bp 3'UTR using the primers VG3_3UTRF and VG3_3UTR_R1. This fragment was TOPO-cloned into pCRII and, after sequencing confirmation, the plasmid was linearized and used as a template for the *in vitro* transcription of digoxigenin-labeled RNA probes using the DIG Labeling Kit (Roche, where). A similar procedure was used for the *vglut1* and *vglut2a/b/c* probes. Probes were purified from the transcription reaction with the

MEGAclear kit (Ambion), quantified by denaturing MOPS-agarose gel electrophoresis, diluted 2X in Hyb+ solution (50% formamide, 5X SSC, 0.1% Tween-20, 50 ug/mL heparin and 5 mg/mL torula RNA) and stored at -20° C until use.

For rescue experiments, *in vitro* transcription of *vglut3*-(CDS+3UTR) and GFP mRNAs was performed with the mMessage mMachine High Yield Capped RNA Transcription Kit (Ambion) using linearized plasmid as a template. Products were purified with Ambion's MEGAclear kit, precipitated and resuspended for injection in 2 mM KCl at 20-250 ng/ul for *vglut3*-(CDS+3UTR) and 5-50 ng/ul for GFP. Again, phenol red was added to a final volume of 5% to act as a tracer.

Microinjection

Injection needles were pulled from 1.2 mm thin wall glass pipettes (World Precision Instruments, Sarasota, FL) on a Narishige PC-10 pipette puller in double-pull mode (temp 1 = 90.1, temp 2 = 80.6). Prior to injection, embryos were collected into injection molds (2% agarose in E3) and oriented with one-cell embryo to the side. Needles were filled with 3-5 ul of MO or mRNA, fitted to a PV820 pneumatic pump (World Precision Instruments) and controlled with a Narishige M152 micromanipulator. MOs and mRNA were injected directly into the yolk sac of 1-cell stage embryos. Injection pressure and time was adjusted to create an injection bolus approximately 1/4 the diameter of the yolk sac.

Whole Mount *In situ* Hybridization

Tü/AB embryos were collected on Day 0 and transferred into E3 containing phenolthiol urea (to inhibit pigmentation) on Day 1. Larva were collected on days 3-5, euthanized with MESAB, and then fixed overnight at 4° C in 4% paraformaldehyde in PBST. The following day, they were washed in PBST (2 x 5 min.) and then either dehydrated in a methanol series (25%/75%, 50%/50%, 75%/25% with PBST, then 100% methanol) for storage at -20° C, or immediately treated with proteinase K at 5 ug/mL for up to 20 minutes and then fixed in 4% PFA for 20 minutes. The larvae were then washed again with PBST (2 x 5 min.) and then prehybridized in Hyb+ for at least 2 hours in a thermomixer (Eppendorf, Westbury, NY) at 65° C, 550-600 rpm. The probe was denatured at 80° C for five minutes, then chilled rapidly on ice. After prehybridization, the Hyb+ was exchanged for 300-500 uL Hyb+ containing 20-200 ng probe, and the larvae were incubated in the thermomixer overnight. The following day, non-specifically bound probe was washed off with 2 x 30 minute washes in 50% formamide/2X SSCT, 1 x 15 minutes in 2X SSCT and 2 x 30 minutes in 0.2X SSCT, all at 65° C in the thermomixer.

For probe detection, larvae were rinsed twice with malate buffer (Roche DIG Wash and Block Buffer Set) and blocked for a minimum of 2 hours in Roche blocking buffer at room temperature. This solution was exchanged for fresh blocking buffer containing anti-DIG Fab fragment conjugated to alkaline phosphatase (Roche) at 1:5000 dilution, and the larvae were incubated overnight at 4° C with gentle agitation. The following day, larvae were washed with malate buffer (6 x 20 min.), rinsed twice with

Roche detection buffer, and incubated in BM Purple Precipitating AP Substrate (Roche) until color stopped developing (typically 3-4 hours). Substrate was washed off with PBST (3 x 5 min.) and the larvae were postfixed with 4% PFA, dehydrated in a methanol series, and transferred to a 2:1 mix of benzylbenzoate:benzylalcohol to clear the yolk.

Larvae were imaged on a Zeiss Axio bright-field microscope using a 10X or 20X air objective. The larvae were transferred to slides resting atop a piece of Whatman filter paper. Rather than using the Hg arc lamp attached to the microscope, illumination was provided via fiber optics from a light box, with the bulbs oriented to provide oblique illumination of the sample. Images were acquired via an AxioCam MRc5 color digital camera using Axiovision software and exported as TIFF files to Adobe Photoshop for analysis.

Whole Mount Immunohistochemistry

Day 5 *asteroid* mutant and sibling larvae were euthanized with MESAB and prefixed in 4% PFA for 10 min. at room temperature, at which time they were transferred to 4° C for a further 24 hours of fixation. This solution was exchanged for 4% PFA + 0.5% Triton-X100, and the larvae were incubated for another 24 h at 4° C. They were then rinsed twice with PBST and blocked with 1X FSGB (0.5% fish skin gelatin, 2% BSA in PBST) for 1-2 h at RT. After blocking, the larvae were incubated with primary antibody diluted in FSGB (1:50 dilution for both α -Ribeye B and α -Otoferlin) for either 3-4 h at RT or overnight at 4° C. Following PBST washes (6 x 20 min.), the larvae were incubated with secondary antibody (Cy5-conjugated goat anti-rabbit, Invitrogen) overnight at 4° C. Larvae were washed again with PBST (6 x 20 min.), then incubated in

a 1:1000 dilution of Alexa 488-conjugated phalloidin (Invitrogen) for 3 hr. at RT and washed again (3 x 20 min).

Larvae were mounted side-down in 4% low-melt agarose on cover slips that were then inverted onto depression slides. Imaging was performed with an Olympus FluoView 300 line-scanning confocal head attached to an Olympus BX51 upright microscope using a 60X (1.4 NA) oil-immersion objective. Excitation wavelengths of 488 nm (Alexa488-phalloiding) and 543 nm (Cy5-conjugated secondary antibodies) were applied, and emitted light was collected through 510-530 nm and 605 ± 12.5 nm barrier filters, respectively. Some bleed-through from the phalloidin staining was observed in the Cy5 channel, but the converse was not the case, and so images were acquired in simultaneous-scan mode with Olympus FluoView software and exported to NIH's ImageJ for analysis.

Electron Microscopy

Day 5 *asteroid* mutant and sibling larvae were euthanized with MESAB and fixed overnight in 3% glutaraldehyde with 1.5% paraformaldehyde in 0.1 M phosphate buffer. After rinsing with 0.1M phosphate buffer, larvae were stained with 1% osmium in 0.1M phosphate buffer for 1 h, rinsed again and dehydrated in an ethanol series (3 x 10 min. washes each of 50%, 80%, 95% and 100% ethanol). The larvae were then washed 2 x 30 min. with propylene oxide and incubated serially in two propylene oxide:araldite mixtures (1:1 and 1:3) before being transferred into 100% araldite for overnight incubation. The following day, the larvae were transferred in araldite to a casting tray, and the araldite was polymerized at 60° C for 48 hours.

Transverse sections were taken through embedded larvae on a microtome with a glass knife. 5 micron sections were taken until just past the eye, then three micron sections were taken into the ear. When the otolith of the anterior macula was visible in one or both ears, the blocks were handed to Jackie DeGagne at the OHRC EM Core for thin sectioning on an RMC MT-7000 ultramicrotome. 60-80 nm thin sections were transferred to a grid for imaging on a Phillips CM100 Electron Microscope. Hair cell ribbons in the ear and neuromasts were imaged at 21,000X – 39,000X magnification.

Images were acquired on an analog camera and negatives were scanned into Adobe Photoshop at 1200 dpi. Image levels were adjusted as necessary to reveal synaptic vesicles close to the ribbon bodies. Vesicles were then counted as described in the text. To measure maximum halo widths and cross-sectional ribbon areas, images were imported into the ImageJ. Halo dimensions were measured by drawing a radial line from the border of the ribbon to the furthest ribbon-associated synaptic vesicle. Ribbon areas were measured by computing the area of a region of interest drawn with the freehand tool around the ribbon. Data (in pixels or pixels²) were exported to Microsoft Excel and converted to metric units.

Statistics

All statistics were computed in Microsoft Excel, and are reported as standard deviations or standard errors of the mean.

3. RESULTS

3.1 Phenotype

The *asteroid* (*ast*) complementation group was isolated from a large scale ENU mutagenesis screen conducted in Tübingen. It displays a classic circler phenotype: no startle response to dish-tapping, an inability to orient to gravity, and a spiraling swim trajectory. Whereas some circlers cannot orient themselves parallel to currents, *ast* mutants perform better in this particular task. The gross morphology of the 120 hpf embryos is normal, although *ast* mutants fail to inflate their swim bladders at a rate higher than siblings. The hair cells of the ear and lateral line organs are also normal. FM 1-43 uptake is comparable to wild-type, indicating normal mechanotransduction (data not shown). Taken together, these phenotypes suggest that the *ast* defect is in hair cell synaptic transmission, or perhaps in central auditory/vestibular circuits.

3.2 Mapping

The *ast* locus was mapped to linkage group 18 of the *Danio rerio* genome. Meiotic mapping with simple sequence length polymorphism (SSLP) markers narrowed the region in which the *ast* locus must lie to a critical interval of approximately 450 kilobases (kb). Two markers, z21330 (total recombinants: 1 out of 246 larvae) and z20981 (total recombinants: 29/1366) defined the northern and southern markers, respectively, of the critical interval. Incomplete assembly of the genome, as well as proximity to the centromere (T. Nicolson, personal communication) precluded further definition of the critical interval.

In the current Ensembl assembly (v44) of the *D. rerio* genome, the *ast* critical interval contains several genes (Fig. 1A). The most attractive candidate in the interval was *vglut3*. Secondary candidates were *cbp90*, *c1q*, and—from a previous release of the assembly (v36)—*eea1* (not shown).

3.3 Sequencing

Using primers designed against the predicted sequences of the 5' and 3' ends of the *vglut3*-CDS, I obtained amplicons from oligo d(T)-primed 1st strand WT and *ast* cDNA (Fig. 1B). cDNA from *ast* mutants yielded two species: one migrating at ~1.6 kb, another at ~1.75 kb. Siblings showed three bands: 1.6, 1.75 and 1.85 kb. Two wild-type strains (Tü and WIK) yielded a single band migrating at 1.85 kb. This pattern was suggestive of an mRNA splicing defect.

The 1.85 kb band was sequenced, and the identity of *vglut3* was confirmed. Alignment of cDNA and genomic sequences reveals 12 exons in the *vglut3* transcript (data not shown). Vglut3 contains 8-10 transmembrane domains, depending on the prediction algorithm (data not shown). Alignments of Vglut3 protein with Vglut1 and 2, as well as an alignment of Vglut3 proteins across species, can be found in the Appendices.

Sequencing of the two mutant and three sibling *vglut3*-CDS bands revealed that the 1.6 kb species is missing exon 2, while the 1.75 kb species contains only a fragment of exon 2 (Fig. 1D). A frameshift results in both cases, such that translation from the cognate mRNAs would generate Vglut3 protein that terminates prior to the first predicted transmembrane domain. The 1.8 kb band from the sibling cDNA library was identical to

that from wild-type Tü and WIK cDNA. Thus, it appears that *asteroid* mutants possess no functional Vglut3.

I next sequenced genomic DNA from *ast* mutants and siblings in the hope of finding a genomic lesion that would cause the splicing defect observed at the mRNA level. The most likely locations would be at the splice-acceptor site at the 3' end of intron 1, the splice-donor site at the 5' end of intron 2, or at the branch-point adenine in intron 1. I sequenced all of these sites in both *ast* mutants and siblings, but detected no mutations (Fig. 1E). The exonic regions of the *vglut3* gene were also identical. Thus, it appears that the genomic lesion may lie in intronic sequence. The sequencing of introns 1 and 2 is currently underway.

3.4 *In situ* Hybridization

I next performed whole mount *in situ* hybridization (ISH) for *vglut3* mRNA in wild-type Tü/AB zebrafish. As shown in Figure 2A, *vglut3* is expressed in ear. Unlike mammalian *vglut3*, there is no staining anywhere in the brain, nor is transcript detected in other tissues where it appears in mammals (e.g. pancreas; data not shown). The signal in the yolk sac is non-specific. Higher magnification reveals *vglut3* in hair cells of the anterior and posterior maculae. The more diffuse staining around these structures may in fact be other suborgans of the ear, but sectioning of stained specimens will be required before further *vglut3*-positive structures can be positively identified. No signal was detected in the neuromasts of the lateral line system.

Next, in collaboration with Nikolaus Obholzer, I examined the distribution of other Vglut isoforms. The CDS of *vglut1* and three isoforms of *vglut2* were cloned and

used to generate ISH probes. The results are shown in Figure 2B. *vglut1* is detected as a diffuse signal in the brain and spinal cord, but not the ear. *vglut2a* and *vglut2b/c* are both detected in complex and overlapping patterns in the CNS, but again, neither is present in the ear, nor in the lateral line. These results indicate that Vglut3 is a hair-cell specific vesicular glutamate transporter.

3.5 Phenocopy

To confirm the identity of *vglut3* as the *ast* gene, I designed three antisense morpholino (MO) oligonucleotides (Fig. 3A): one against the *vglut3* start codon (VG3-ATG), and two that are predicted to interfere with the correct splicing of exon 2 (VG3-X2del and VG3-X2del2). Together with Robert Duncan, these were injected into the yolk sacs of one-cell stage Tü/AB (wild-type) embryos. These embryos were then grown up to day 5 and screened for deafness and balance defects.

All three MOs generated a dose-dependent balance defect in Tü/AB larvae (Fig. 3C). Spiraling swim-trajectories were observed in some, though not all, balance-defective morphants, but the startle response was intact. The dose-response curve in Fig. 3C shows results from duplicate experiments in most cases, though some concentrations (e.g. VG3-x2del at 250 uM) have only been injected once. Replicate trials are underway for all under-represented experiments. Control morpholinos with 5 base-pair mismatches had no effect at any dosage (data not shown).

Figure 3B shows *vglut3*-CDS cDNA amplicons derived from mRNA extracted from VG3-X2del and VG3-X2del2 morphants. Both MOs caused apparent splicing defects, though wild-type bands at 1.8 kb are present, indicating that the MOs were not

completely effective in disrupting *vglut3* pre-mRNA splicing. Both VG3-X2del and -X2del2 returned 1.6 kb bands that co-migrate with the 1.6 kb band from *ast* mutant and sibling mRNA, while a 1.75 kb band was returned only by VG3-X2del2. This MO also returned an amplicon at ~1.4 kb. Sequencing of the amplicons derived from *vglut3* morphants is in progress.

3.6 Rescue

I attempted to rescue the *asteroid* phenotype with *in vitro* transcribed *vglut3* mRNA, including the 8 nt of 5' UTR and the complete CDS and 3' UTR. I co-injected this mRNA into the yolk of one-cell *asteroid* embryos along with GFP mRNA at a 10:1 molar ratio. GFP-positive larvae were separated out from the clutch and grown to Day 5, but ~25% of the survivors displayed the *asteroid* phenotype (data not shown). As this experiment was conducted prior to obtaining the 5' UTR of *vglut3* and has not been repeated since, I cannot say whether exogenous *vglut3* mRNA was translated efficiently, if at all.

3.7 Immunohistochemistry

Because neither *vglut1* nor *vglut2b/c* are present to compensate for the loss of *vglut3* in *asteroid* mutants, one would expect (a) that synaptic vesicles (SVs) in mutant hair cells are empty of glutamate and (b) that the hair cell afferent synapse is functionally silent. Two direct ways to test this are by recording microphonic potentials in the VIIIth cranial nerve and calcium-imaging in the statoacoustic ganglion. The former technique is currently being set up in the Nicolson Lab, and the latter is in the pilot stage. At present,

however, I have examined WT and *vglut3*^{-/-} larva for possible secondary effects of a silent synapse.

To determine whether a homeostatic mechanism is operating in *vglut3*^{-/-} hair cells, I examined the subcellular distribution of hair cell presynaptic proteins: Ribeye B and Otoferlin. I reasoned that the hair cell might attempt to compensate for its defective transmission by increasing the number of ribbon bodies (as assessed by Ribeye B staining) and/or increasing the recruitment of SVs to existing ribbons. Otoferlin, a putative Ca²⁺-sensor for hair cell SVs, was used as a vesicle marker.

In all cells, ribbons abut the basal plasma membrane. In general, hair cells in the ear have more Ribeye B puncta than do those of the neuromasts (Fig. 4). I have not yet made a quantitative survey, but my preliminary “eyeball” estimate is that ear hair cells have 6-9 ribbons each, while neuromast hair cells have 3-5. There is no difference between *vglut3* mutants and their WT siblings.

Otoferlin’s status as a hair cell SV marker was supported by a recent report showing its enrichment at the basal plasma membrane (Roux et al., 2006). However, in my hands, our antibody against the *D. rerio* Otoferlin reports a uniform PM distribution, with no obvious enrichment at the basal pole of the cell (Fig. 5). This is consistent with other reports of Otoferlin distribution (Brandt et al., 2007). Again, while these results are not quantitative, there does not appear to be any difference in Otoferlin distribution between *vglut3* mutants and their wild-type siblings.

3.8 Ultrastructure and Morphometry

In a recent study of *vglut1* knockout mice, it was reported that the reserve pool of synaptic vesicles at some central synapses was depleted by about 50% (Fremeau et al., 2004b). I wondered whether a similar phenotype would be found in *vglut3* *-/-* hair cells. Together with Nikolaus Obholzer, I analyzed hair cells afferent terminals in WT and *vglut3* *-/-* ears and neuromasts by transmission electron microscopy.

The ultrastructure of the zebrafish hair cell ribbon synapse is schematized in Figure 6A. The typical ribbon body is an electron-dense sphere surrounded by a filamentous halo that is decorated with synaptic vesicles. In sections that happen to include the plasma membrane, one occasionally observes small, dense pod-like structures that appear to anchor the ribbon body at the active zone.

I adopted the following criteria in scoring the number of ribbon-associated SVs: (1) a vesicle must directly appose the ribbon-halo; (2) it must be well-formed (i.e. have a roughly circular cross-section); and (3) it must have a diameter of 30-50 nm (Schnee et al., 2005). These criteria exclude the recycling pool of SVs—as well as any endosomal intermediates that may happen to occur near the ribbon body—and are meant to confine my analysis only to SVs already recruited to the ribbon.

Representative sections through WT and *vglut3* *-/-* ribbons are shown in Figures 6B and 6C. In both cases, the ribbon body is well formed and lies just above the presynaptic active zone. The halos extend 50-100 nm from the ribbon body. While there is no difference in cross-sectional ribbon area or maximum halo width between WT and mutant synapses, ribbon bodies in hair cells from *vglut3* *-/-* hair cells show a ~60% decrease in SV decoration (Fig. 6D). Cumulative probability curves (Fig. 6G) show that half of all *vglut3* *-/-* ribbons have fewer than 4 SVs per cross-section, as compared to 11

for WT ribbons. In many *vglut3* ^{-/-} sections, smaller (diameter <30 nm) and/or more tubular vesicular structures can be seen at or near the ribbon halo (data not shown), but these were excluded from the present analysis.

The decrease in ribbon-associated vesicles may reflect a defect in recruitment or a defect in SV biogenesis per se. Counting of vesicles in the recycling pool (a zone 100-300 nm away from the ribbon) may help distinguish between these possibilities, and is already underway.

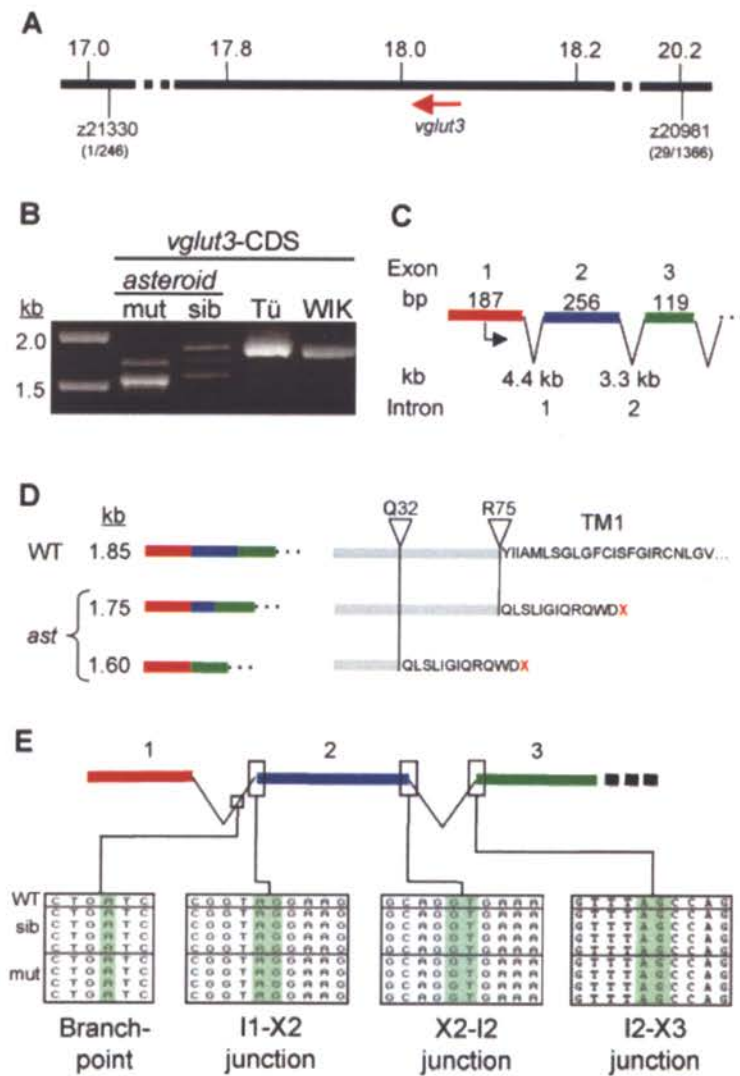


Figure 1. Cloning and sequencing of *vglut3*. (A) A schematic of the *asteroid* critical interval with the position of the *vglut3* gene and defining markers indicated in megabases. The number of recombinants is given below the markers. (B) cDNA amplicons obtained with *vglut3* primers flanking the CDS. (C) Genomic structure through the first three exons of *vglut3*. (D) mRNA and protein structures of WT and *ast* forms of *vglut3*. Premature stop codons are indicated by a red “X.” (E) Genomic sequencing data from likely locations for the *ast* lesion, with relevant bases highlighted in green. Four replicates from *ast* siblings and mutants are compared against wild-type Tü sequence.

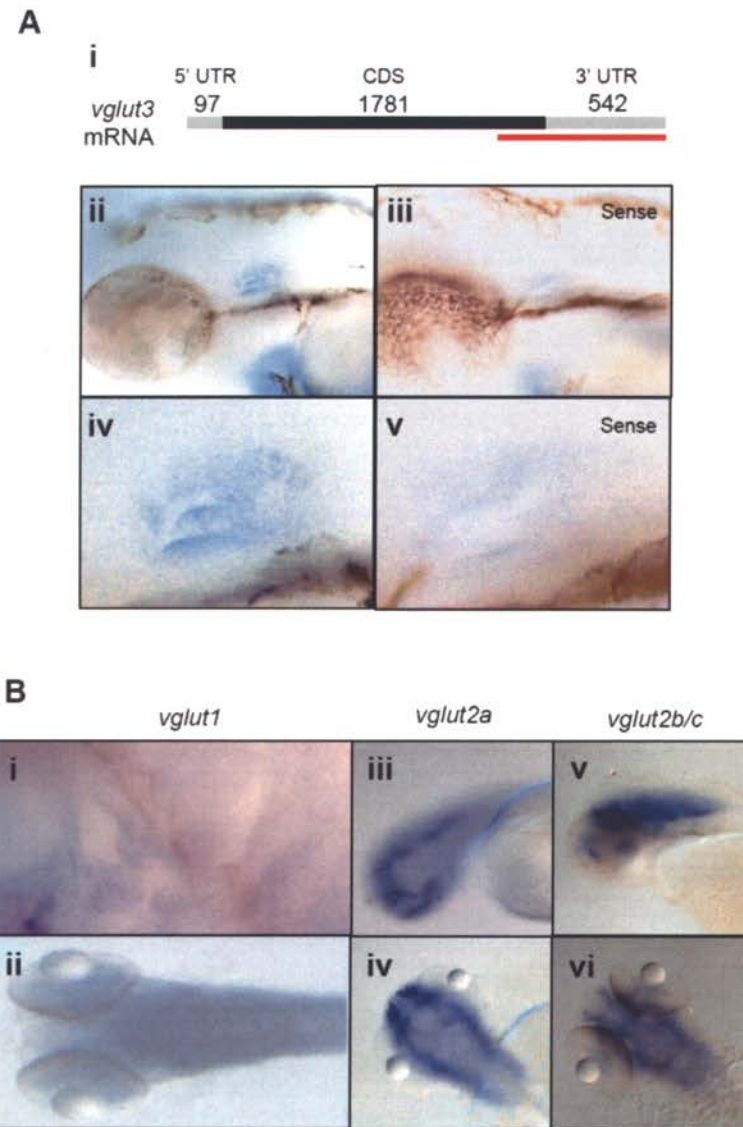


Figure 2. *In situ* hybridization against *vglut3* mRNA. (Ai) A schematic of full-length *Vglut3* mRNA with the location of the *in situ* probe indicated in red. (Aii) Results with the antisense probe showing *vglut3* mRNA in the ear (blue). The yolk sac staining is non-specific. (Aiii) Sense control. (Aiv-v) Enlargements of Aii and Aiii, respectively. (Bi-vi) ISH against other *Vglut* isoforms, showing intense brain staining, but no signal in the ear. Bi shows an enlargement akin to Aiv. All images are oriented with anterior to the left. Panel Bii from Smear et al., 2007.

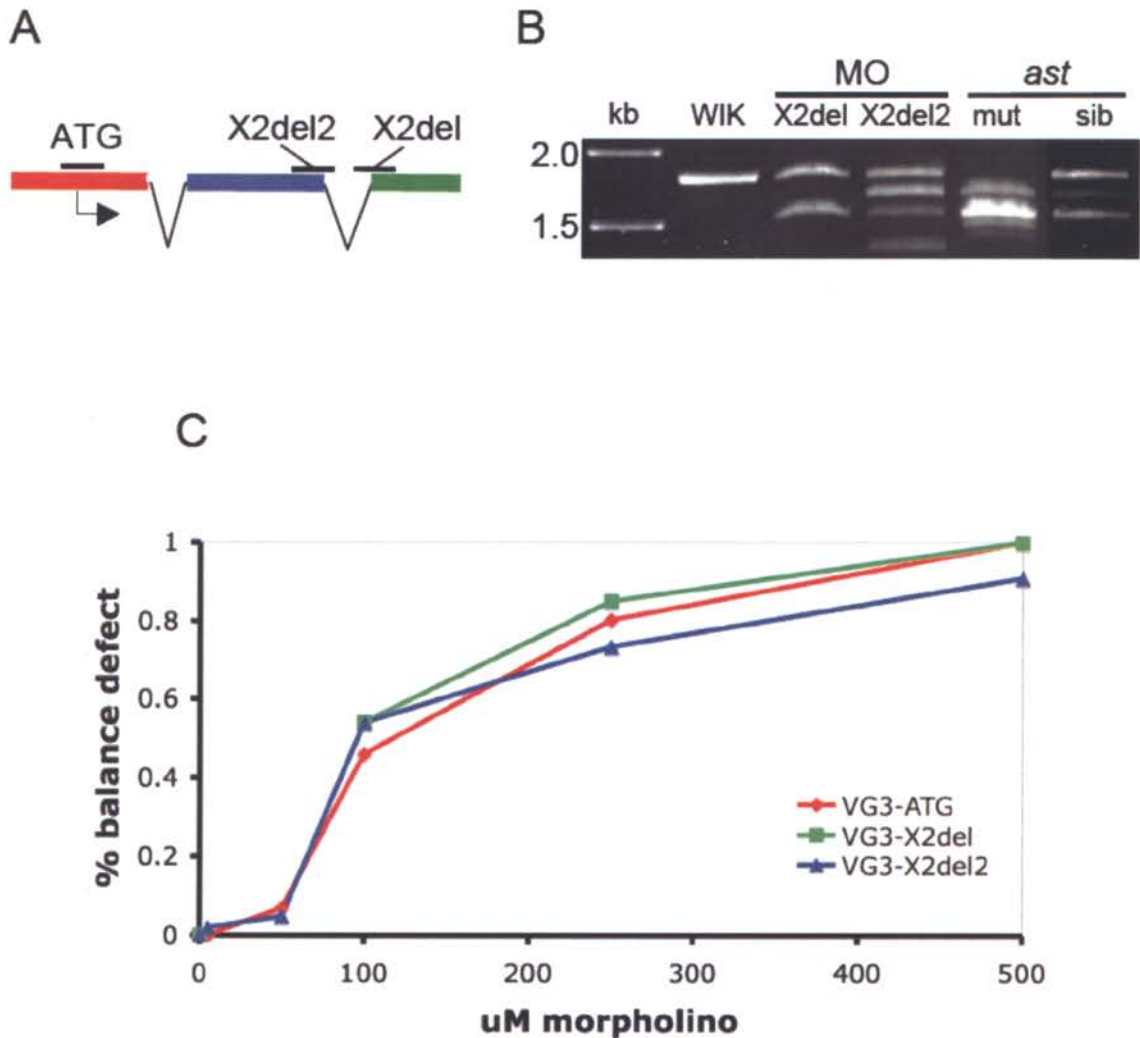


Figure 3. *vglut3* morpholinos induce a balance defect in Day 5 Tü/AB larvae. (A) Locations of the sites against which the indicated MOs were designed. (B) Amplicons derived from cDNA from Day 3 VG3-morphants and *ast* mutants and siblings. The contrast of the *ast* sib lane has been adjusted to reveal all amplicons. (C) A dose-response curve for the three MO used in this study. All larvae were screened for balance defects on Day 5. The control MOs had no effect (data not shown).

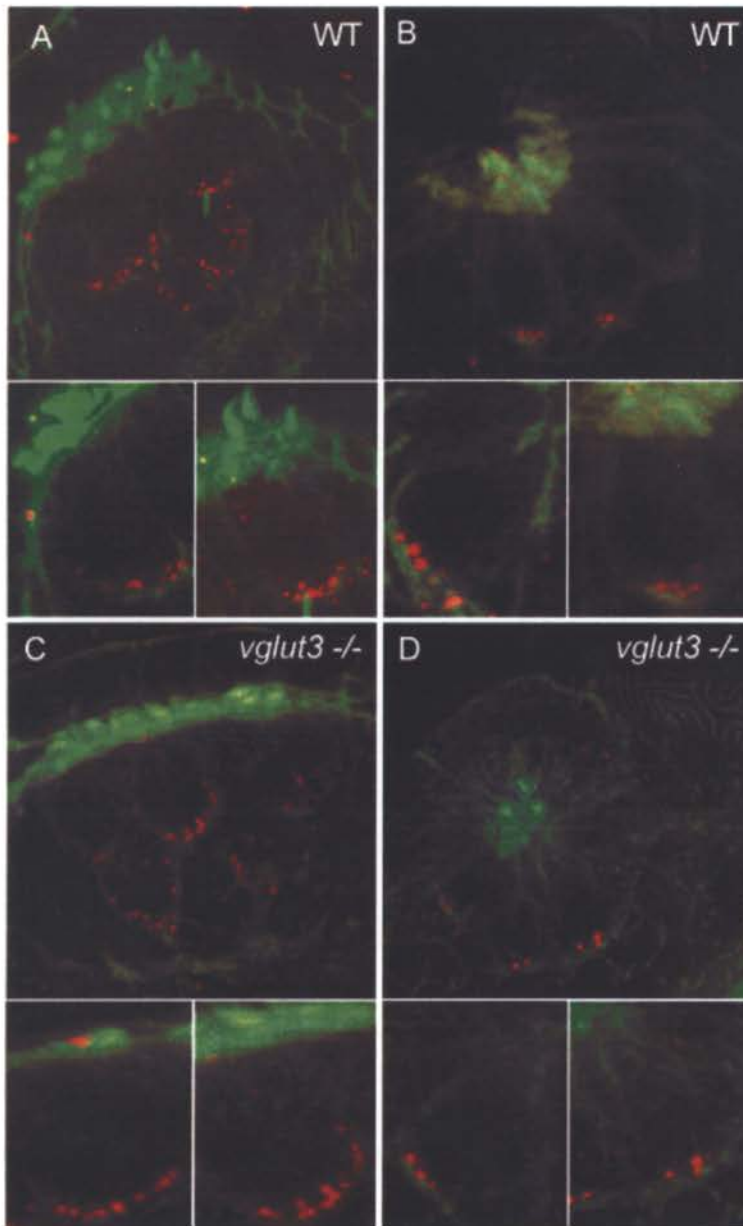


Figure 4. Ribeye B distribution in WT and *vglut3* -/- hair cells. Maximum-intensity projections through cristae (A and C) and neuromasts (B and D) from Day 5 WT and *vglut3* -/- fish, with enlargements of individual hair cells (smaller panels). Actin was stained with Alexa488-conjugated phalloidin (green) to outline the cell bodies; Ribeye B was detected via a Cy5-conjugated 2^o antibody (red).

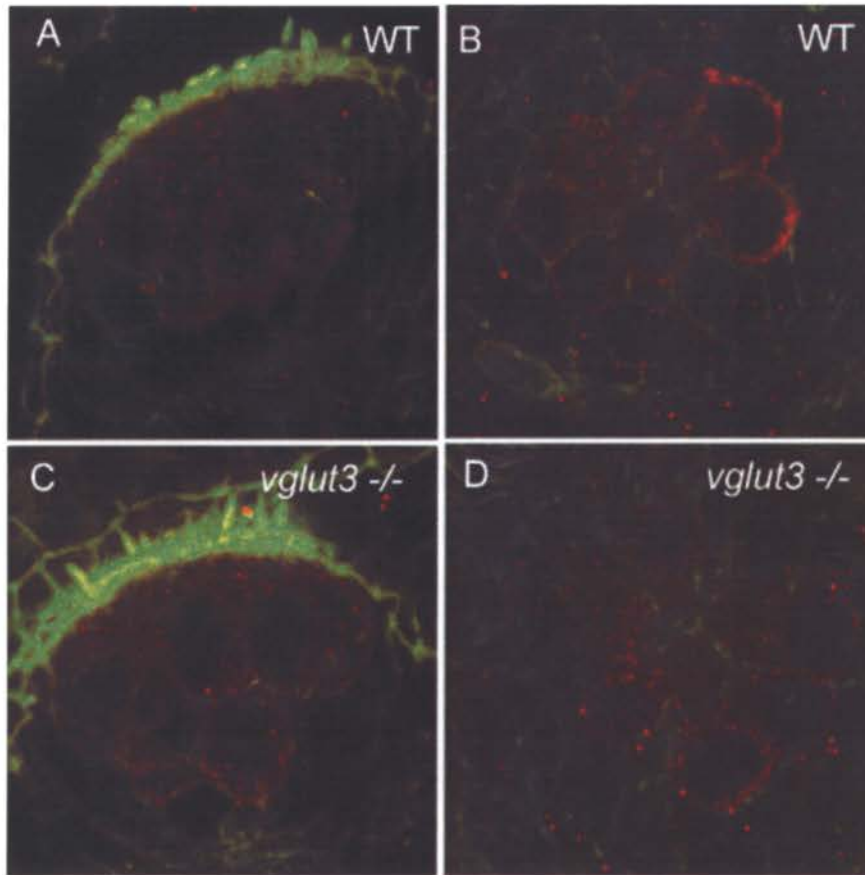


Figure 5. Otofelin distribution in WT and *vglut3* -/- hair cells. Maximum-intensity projections through cristae (A and C) and neuromasts (B and D) from Day 5 WT and *vglut3* -/- fish. Actin was stained with Alexa488-conjugated phalloidin (green) to outline the cell bodies; Otofelin was detected via a Cy5-conjugated 2^o antibody (red).

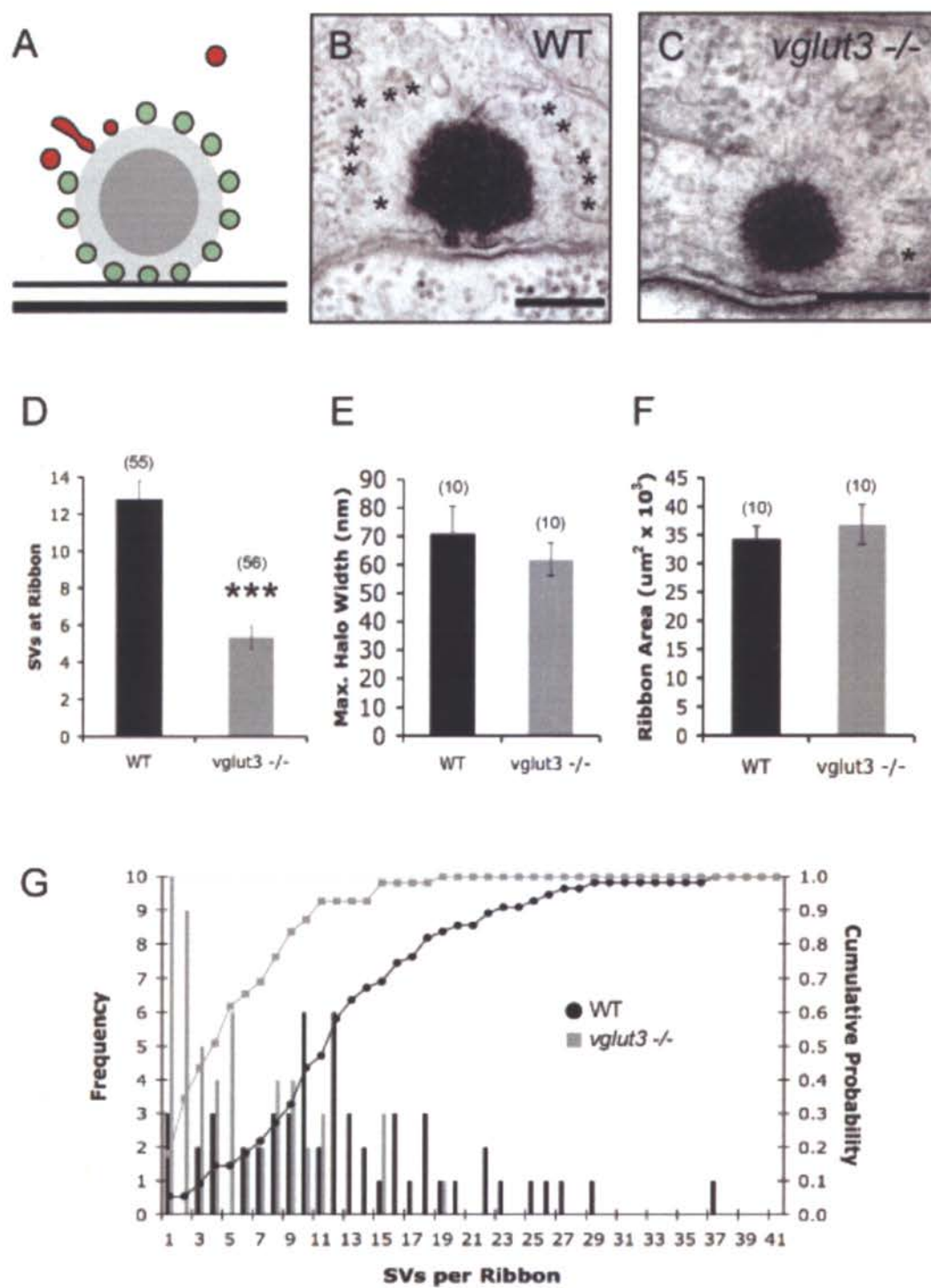


Figure 6. see legend on next page

Figure 6 (previous page). Ultrastructure and morphometry of WT and *vglut3* ^{-/-} ribbon synapses. (A) A schematic of the ribbon synapse showing the ribbon body (dark gray), the ribbon halo (light gray), scorable synaptic vesicles (green) and vesicles disqualified on the basis of size, shape or distance from the halo (red). (B) A ribbon synapse from a WT hair cell with 12 SVs at the border of the halo. (C) A ribbon synapse from a *vglut3* ^{-/-} hair cell with just one ribbon-associated SV. (D) WT ribbons coordinate 12.8 ± 1.0 SVs, while *vglut3* ^{-/-} ribbons coordinate just 5.34 ± 0.6 (***, $p < 0.001$, Student's t-test). There was no significant difference in maximum halo width (E; 71.1 ± 9.6 nm in WT, 61.8 ± 5.9 in *vglut3* ^{-/-}) or in the cross sectional ribbon areas (F; $3.44 \pm 0.21 \times 10^4 \mu^2$ for WT, $3.68 \pm 0.34 \times 10^4 \mu^2$ for *vglut3* ^{-/-}) between WT and *vglut3* hair cells. (G) Frequency histogram (bars) and cumulative probability curves for SV counts at WT and *vglut3* ^{-/-} synapses.

4. DISCUSSION

The data presented in this thesis collectively identify *vglut3* as the gene mutated in the *asteroid* circler mutants and point to a role for Vglut3 in hair cell synaptic transmission and synaptic vesicle recycling/biogenesis.

While the *ast* lesion has not yet been identified at the genomic level, four key findings of this work support the candidacy of *vglut3*: (1) the deletion of all or part of exon 2 correlates with the *ast* phenotype; (2) *vglut3* expression is found only in the hair cells of the ear, and not in neurons of the CNS; (3) morpholinos directed against the start codon and splice sites of *vglut3* cause balance defects in wild-type fish; and (4) *ast* mutants show a reduction in ribbon-associated synaptic vesicles, a finding that corresponds with the phenotype of *vglut1* knockout mice (see below).

4.1 Mis-splicing of *vglut3* mRNA

Two mutant species of *vglut3* mRNA were found in this work. In one, exon 2 is completely deleted; in the other, exon 2 is only partially deleted. This latter species is likely the result of a weak splice acceptor site in the middle of exon 2 that is usually dominated by the one at the end of intron 1. That the genomic lesion does not reside at the conserved intronic splice-sites was unexpected, but there are other pre-mRNA elements that can influence splicing patterns. These elements can reside in both exons and introns, and can both enhance or inhibit splicing (Cartegni et al., 2002; Matlin et al., 2005). Analysis of *vglut3* cDNA with an exonic splicing enhancer prediction program (ESEfinder: rulai.cshl.edu/tools/ESE (Cartegni et al., 2003; Smith et al., 2006)) revealed

the presence of several putative ESEs in exon 2, but none of them were altered in *vglut3* *-/-* mutants (data not shown). A more likely location for the *ast* lesion is in one of the introns flanking exon 2. I have yet to make a survey of predicted enhancer/silencer sites in this sequence (a total of 8 kb), but it is possible that such a site, if it exists, carries a disrupting point mutation.

Another possibility is that the *asteroid* mutation does not disrupt a regulatory element per se, but somehow alters the secondary structure of the *vglut3* transcript in such a way that the splicing elements required for faithful exon 2 inclusion are occluded. Precedent for this sort of regulation can be found in *MAPT*, the human form of tau, where mutations in intron 9 disrupt a secondary structure that affects the alternative splicing of exon 10, altering the ratio of 4R-tau to 3R-tau and leading to frontotemporal dementia and Parkinsonism (Varani et al., 1999). A test of this hypothesis would require intronic sequence of *vglut3* pre-mRNA and the use of an RNA secondary structure prediction program such as Mfold (Mathews et al., 1999; Zuker, 2003). The complete sequencing of *vglut3* introns 1 and 2 is underway.

The partial or complete deletion of exon 2 from *vglut3* mRNA would result in a protein that terminates before synthesis of the first transmembrane domain, thus rendering a functionally inactive protein. The frameshift-generated premature stop codon (PTC) is expected to activate nonsense-mediated decay (NMD) mechanisms in *vglut3* *-/-* hair cells, sequestering and eventually eliminating both mutant forms of *vglut3* mRNA (Conti and Izaurralde, 2005). Confirmation for NMD of mutant *vglut3* transcripts awaits ISH results from *ast* mutants and siblings.

4.2 *vglut3* Distribution

The *in situ* hybridization results presented in this thesis localize *vglut3* mRNA exclusively to hair cells in the ear. No transcript was detected in the brain, nor in the kidneys or liver (data not shown), data which stand in contrast to *vglut3* expression in mice and rats as reported by a number of groups (Fremeau et al., 2002; Gras et al., 2002; Schafer et al., 2002; Takamori et al., 2002). Whether this is the result of the particularity of the zebrafish *vglut3* promoter is unknown, but there is reason to believe that my ISH protocol has not yet been fully optimized: the lack of *vglut3* staining in hair cells of the lateral line organs. No transcript for any of the five *vglut* isoforms tested was seen in neuromasts, the hair cells of which are presumed to be highly similar—if not identical—to those of the ear. Assuming that this similarity extends at least as far as their neurotransmitter profile, I would expect them to test positive for at least one of the Vgluts. The quality of my protocol for enabling detection in neuromasts could be tested by performing ISH for a known markers of neuromasts, such as *eyal* (Grant et al., 2005); only if our current protocol works with these probes can we reasonably conclude that these organs do not express any of the known Vgluts.

The above discussion notwithstanding, *vglut3* *-/-* fish are able to orient themselves to the direction of current flow when their dishes are swirled. Since the lateral line system is specialized to detect current flow, it is possible that the lack of *vglut3* mRNA in neuromasts is a bona fide result. Furthermore, our ISH for *vglut1* and *vglut2a/b/c* reproduce previous findings (Smear et al., 2007), indicating that our protocol is adequate for detection in the brain, and that *vglut3* mRNA is indeed absent from the zebrafish CNS.

The absence of Vglut1 mRNA in the zebrafish ear stands in contrast to a report that Vglut1 is present in IHCs of the guinea pig cochlea (Furness and Lawton, 2003). The polyclonal antibody used in this study was raised against aa 456-560 of rat Vglut1, a region that shows 62% identity and 72% similarity with rat Vglut3 (data not shown). At the time of this study, the Vglut1 knockout mouse (Fremeau et al., 2004b) had not been reported, and no other specificity controls (e.g. preabsorption with recombinant antigens from any of the Vgluts) were reported in this study. Therefore, while Vglut1 may indeed be present in these cells, Vglut3 cannot be ruled out.

In the mammalian CNS, Vglut3 is coexpressed in subsets of cholinergic, serotonergic and GABAergic neurons (Fremeau et al., 2002; Gras et al., 2002), thus raising the possibility that these neurons release co-release glutamate with these other neurotransmitters. The reciprocal possibility is that hair cells may release neurotransmitters other than glutamate. ISH and IHC for other neurotransmitter markers such as choline acetyltransferase and tyrosine hydroxylase would be a simple way to determine if this is the case.

A rabbit polyclonal antibody against Vglut3 is currently being generated. Immunodetection of Vglut3 protein (using *asteroid* mutants as negative controls) will allow confirmation of the ISH results presented here, allow us to determine the subcellular localization of Vglut3, and may eventually serve as a marker capable of distinguishing bona fide synaptic vesicles from their endosomal intermediates and precursors.

4.3 Phenocopy

Morpholinos directed against the *vglut3* start codon (to inhibit translation) and the splice-sites of intron 2 (to promote skipping of exon 2) cause a balance defect in wild-type Tü/AB zebrafish. The MO-induced phenotype is weaker than the *asteroid* phenotype, and indeed, when *vglut3*-CDS was amplified from VG3-X2del and VG3-X2del2 morphants, a significant fraction of wild-type *vglut3* mRNA was seen to have been spared.

The high penetrance of balance-defect phenotype suggests that hair cells in the ear are consistently loaded; that is, injection into the yolk of 1-cell embryos is sufficient to deliver MOs to these cells, and they remain active up to screening on Day 5. Thus, my results are not explained by a mosaic distribution of VG3-MOs to larval hair cells. However, it is possible that the absolute quantity of MOs delivered to each hair cell may not have been high enough to saturate the extant *vglut3* transcript. If a fraction of *vglut3* mRNA eludes the VG3-MOs, then some amount of wild-type Vglut3 protein will be produced. This reduced pool of Vglut3 may be sufficient to support transmission in hair cells of the posterior macula, where hearing occurs. The ambient environment in which our larvae are housed is quiet, and zebrafish themselves do not vocalize. Therefore, these auditory hair cells may have lower stimulus loads than their vestibular neighbors, which would explain why morphants can still exhibit a startle response.

The highest injected concentration reported here, 500 μ M, is sufficient to confer a balance defect to greater than 90% of injected fish, but injections of 1 mM MOs have proven toxic, with more than 50% of injected clutches dying by 48 hpf, and a majority of the survivors displaying severe morphological phenotypes such as dorsalization.

Furthermore, due to variations in needle-tip diameter and injection pressure, injection-bolus size was only approximately constant across experiments. Thus, it is possible that injections of 1 mM MOs delivered more than twice what was delivered by injection of 500 μ M. Further refinement of the injection technique may reveal an optimal concentration that causes a more severe phenotype without being unduly toxic.

vglut3 morphants have normal hearing as assessed by the dish-tapping startle response assay. However, this assay may not be well suited to detecting weak auditory phenotypes. In our current protocol, larvae are removed from the quiet of their incubator, transferred to a benchtop, and the rim of the petri dish is tapped lightly with a metal probe (or, in many cases, a Sharpie permanent marker) at highly variant rates (say roughly 3-5 bursts, at 0.5-3 Hz, at 5 to 30 second intervals, for 5 to 15 minutes). Wild-type larvae will respond to taps for a few minutes, after which the startle-response seems to adapt. After a brief resting period in the incubator, the response returns. The time course of adaptation and recovery has not been measured in any rigorous way, but doing so may provide a benchmark against which to compare the behavior of mutants such as *comet*, which also have an impaired, though not eliminated, startle-response (N. Obholzer, personal communication), and may also reveal an auditory phenotype in *vglut3* morphants. This experiment would require a more sophisticated method of delivering sound stimuli, with controls for both amplitude and frequency, as well as a method for scoring startle responses within a large group of larvae. Some inspiration for the design may be taken from other kinematic analyses of zebrafish motility (Masino and Fetcho, 2005; McLean et al., 2007; Smear et al., 2007).

4.4 No Compensatory Increase in Ribbon Number or Size

The Ribeye B IHC (Fig. 4) and measurements of ribbon cross-sectional area (Fig. 6F) reported above show that there is no difference in either parameter between WT and *vglut3* *-/-* hair cells. In this respect, the synapses themselves can be considered “mature,” even if the synaptic vesicles themselves are not (see below). Immature ribbon synapses in the mouse cochlea display supernumerary ribbon bodies (Sobkowicz et al., 1982), even at the same active zone (Sendin et al., 2007), a finding not recapitulated here at either the light or electron microscopic levels. That the synapses appear normal (other than the relative paucity of SVs) in hair cells that presumably cannot drive activity in the afferent neurons of the VIIIth cranial nerve suggests that transmission is not required for the development or maintenance of the ribbon body. Furthermore, it suggests that ribbon components traffic to the presynaptic active zone along a different pathway than do synaptic vesicles.

4.5 Synaptic Vesicles at the Hair Cell Ribbon Synapse

The synaptic ribbon is thought to facilitate and sustain high-frequency SV exocytosis in auditory hair cells (see Introduction for more detail). Whatever the mechanism by which this is accomplished, a first step must be the recruitment of SVs to the ribbon. In *vglut3* *-/-* hair cells, this step appears to be disrupted.

On average, thin (60-80 nm) sections through wild-type ribbon synapses revealed 12.8 ribbon-associated SVs, compared to 5.3 SVs at *vglut3* *-/-* ribbons. The value of ~13 SV/ribbon compares with hair cell ribbons from other species: using my counting methodology, the mouse ribbon in Figure 2H of Sendin et al., 2007, coordinates 13 SVs;

that in Figure 2B of Schnee et al., 2005, coordinates 9; and the mammalian ribbons in panels e, f, g, j, and l from Figure 1 of Moser et al., 2006, coordinate an average of 11. (These authors did not count the number of ribbon-associated SVs in these figures, so I cannot say how my values compare to theirs.) When applied to the bullfrog sacculus hair cell in Figure 1A of Lenzi et al., 1999, 34 vesicles are counted, but this is likely a consequence of the large ribbons in this cell type.

The consistency of these counts compared across species, and with slight differences in fixation and image acquisition, indicates that any error in my counts are the result of my counting criteria, and not our EM protocol. I believe my criteria are valid, as they are based on a rigorous survey of SV characteristics in turtle hair cells (Schnee et al., 2005) Furthermore, any error in my measurements is consistently applied across both *vglut3* *-/-* and wild-type ribbons, so the statistical significance of their comparison is likely still valid.

This finding extends results obtained in central synapses from *vglut1* knockout mice, which displayed a similar reduction in SVs within 300 nm of the active zone (Freneau et al., 2004b) and implies a role for Vglut3 in the recruitment of SVs to the ribbon, or in SV recycling/biogenesis, or both. Each implication is based on the premise that the presence of an NT transporter fundamentally distinguishes a synaptic vesicle from an endosome or any other small organelle.

4.5.1 SV Recruitment

The molecule(s) tethering SVs to ribbon bodies have not been identified. The filamentous structures between SVs and the ribbon likely reside at the ribbon, as they are present there even when SVs are not and are not visible on SVs in the reserve pool; however, they must physically interact with some protein(s) of the SV. From a quality-control point of view, it only makes sense for ribbons to recruit signaling-competent vesicles; that is, vesicles that are filled with neurotransmitter. I therefore submit that Vglut3, as the sole glutamate transporter in hair cells of the zebrafish ear, may physically interact with the filaments of the ribbon halo.

The membrane topology of Vglut3 has not yet been determined, but as the N- and C-termini of Vglut2 are predicted to reside in the cytoplasm (Jung et al., 2006), and given their high degree of sequence similarity (see Appendix), the same is probably true of Vglut3. There are 98 amino acids N-terminal to the first predicted transmembrane domain, and 83 C-terminal from the last. Even if a component of the ribbon halo is not found, it is probable that one will find other interactors and regulators of Vglut3, a subject about which precious little is known.

4.5.2 SV Biogenesis and Recycling

At some point, signaling-competent SVs must be synthesized de novo or reformed from their endocytic intermediates. While many SVs at both conventional and ribbon synapses are likely products of local recycling, the stoichiometric presence of certain endosomal proteins (e.g. Vti1a β) on SVs means that de novo SV biogenesis begins at the trans-Golgi or an endosomal compartment not too far downstream (Sudhof, 2004). This

is not surprising, since the same can be said of all secretory vesicles and, indeed, all PM transmembrane proteins. However, considering that SVs require not only neurotransmitter (i.e. a NT transporter and a proton-pump), but also the appropriate v-SNARE (synaptobrevin) and its interactors (synaptophysin), a Ca^{2+} sensor (synaptotagmin at conventional synapses and perhaps otoferlin in hair cells), and a host of other components (Sudhof, 2004), one begins to appreciate that SVs are defined combinatorially, and not by any one protein. Even if SV maturation occurs on site (perhaps by recruitment of components that were trafficked separately), SV precursors must be selected at an early point in their biogenesis and sent along the appropriate transport pathways to the synapse. It is possible that NT transporters, alone or in conjunction with other obligatory proteins, specify SV precursors at the trans-Golgi or nearby early endosomes.

A similar quality-control mechanism may operate during recycling of SVs from endosomal compartments at or near the synapse. (Reuse models such as “kiss-and-stay” do not require fresh repackaging of SVs.) In the endosomal recycling model, SVs fully fuse with the PM during exocytosis and their constituent proteins diffuse laterally through the PM. These proteins are recovered in endocytic vesicles (through clathrin-dependent and -independent mechanisms), which are then trafficked to an early endosome, from which new SVs are generated and returned to the active zone. How endocytosis of individual proteins is related to the recycling or reformation of SVs is controversial. Some groups have reported extensive mixing of exocytosed SV proteins in the PM (Fernandez-Alfonso et al., 2006; Wienisch and Klingauf, 2006), while at least one has reported that molecules of synaptotagmin, the SV calcium sensor, form clusters that are

exo- and endocytosed together (Willig et al., 2006). Whatever the case, recycled SVs must be able to release NT in an activity-dependent manner, and so some mechanism of quality control, perhaps requiring on an NT transporter, must be active.

A key set of future experiments would be to determine what SV proteins are present on the few vesicles that do manage to arrive at the ribbon in *vglut3* mutants. Functionally, NT transporters are most dependent on the vacuolar proton pump, but these complexes are found on lysosomes and other organelles. Are NT transporters required to recruit them to nascent SVs? If so, one would expect them to be absent in *asteroid* fish. Not that I propose to survey all known SV proteins in this way: if the proton pump, synaptotagmin and/or otoferlin, synaptobrevin and synaptophysin are present, this may be enough to reasonably discard this hypothesis. However, if one or more of them is missing, the *asteroid* mutant background may provide an excellent platform on which to test key questions about hair cell SV biogenesis and recycling in an intact, living organism.

4.6 Future Directions

The findings presented in this thesis open several potentially promising lines of investigation. Foremost is how Vglut3 is involved in getting SVs to the ribbon body. To gain insight into this question, I propose the following series of experiments:

1. Counting of SVs in the reserve pool in WT and *vglut3* *-/-* synapses. If SVs are found to be depleted in the zone 100-500 nm away from the ribbon body, this would lend support to the biogenesis/recycling hypothesis.

Alternatively, if SVs traffic normally to this pool, this would favor the recruitment hypothesis.

2. Further characterization of SVs in *vglut3* $-/-$ hair cells. A more thorough morphometric analysis of the synaptic region may shed light on distribution of SVs among the three pools (reserve, recycling and readily-releasable). Also, a survey of the proteins present on SVs at mutant synapses would help dissect Vglut3's role, if any, in SV biogenesis.
3. Transient, and eventually transgenic, rescue of *asteroid* with Vglut3-GFP. If the tagged protein rescues the *ast* phenotype, then it may also serve as a marker of bona fide SVs. In any event, it is important to determine when and where Vglut3 enters the transport pathway to the ribbon synapse.
4. Transient or transgenic rescue of *asteroid* with WT and N/C-terminal deletions of *vglut3*. These two cytodomains may have different functions, or one or the other may be dispensable. In either case, there will be a rational basis for the design of the fifth experiment.
5. A yeast two-hybrid screen with the N- and/or C-terminal cytodomains of Vglut3. The identification of Vglut3 binding proteins may aid in placing the NT transporter within an SV biogenesis/recycling pathway. Alternatively, it may shed light on what proteins are involved in tethering SVs to the ribbon body.

6. SUMMARY

The data presented in this thesis collectively identify *vglut3* as the gene mutated in the *asteroid* circler mutants and point to a role for Vglut3 in hair cell synaptic transmission and synaptic vesicle recycling/biogenesis. While the *ast* lesion has not yet been identified at the genomic level, four key findings of this work support the candidacy of *vglut3*: (1) the deletion of all or part of exon 2 correlates with the *ast* phenotype; (2) *vglut3* expression is found only in the hair cells of the ear, and not in neurons of the CNS; (3) morpholinos directed against the start codon and splice sites of *vglut3* cause balance defects in wild-type fish; and (4) *ast* mutants show a reduction in ribbon-associated synaptic vesicles. These results suggest a role for Vglut3 in the hair cell synaptic vesicle cycle, either in biogenesis/recycling or in the recruitment of vesicles to the synaptic ribbon. That there is no compensatory increase in the number of ribbons in *vglut3* *-/-* hair cells suggests that the hair cell afferent synapse develops in an activity-independent manner, though the contribution of efferent innervation of hair cells was not addressed in this study. The *asteroid* mutant thus provides a platform on which to investigate the role of neurotransmitter transport in hair cell synaptic biology.

7. REFERENCES

- Adato A, Lefevre G, Delprat B, Michel V, Michalski N, Chardenoux S, Weil D, El-Amraoui A, Petit C (2005) Usherin, the defective protein in Usher syndrome type IIA, is likely to be a component of interstereocilia ankle links in the inner ear sensory cells. *Hum Mol Genet* 14:3921-3932.
- Ahmed ZM, Goodyear R, Riazuddin S, Lagziel A, Legan PK, Behra M, Burgess SM, Lilley KS, Wilcox ER, Griffith AJ, Frolenkov GI, Belyantseva IA, Richardson GP, Friedman TB (2006) The tip-link antigen, a protein associated with the transduction complex of sensory hair cells, is protocadherin-15. *J Neurosci* 26:7022-7034.
- Bai L, Xu H, Collins JF, Ghishan FK (2001) Molecular and Functional Analysis of a Novel Neuronal Vesicular Glutamate Transporter
10.1074/jbc.M104578200. *J Biol Chem* 276:36764-36769.
- Bellocchio EE, Reimer RJ, Fremeau RT, Jr., Edwards RH (2000) Uptake of glutamate into synaptic vesicles by an inorganic phosphate transporter. *Science* 289:957-960.
- Bellocchio EE, Hu H, Pohorille A, Chan J, Pickel VM, Edwards RH (1998) The localization of the brain-specific inorganic phosphate transporter suggests a specific presynaptic role in glutamatergic transmission. *J Neurosci* 18:8648-8659.
- Brandt N, Kuhn S, Munkner S, Braig C, Winter H, Blin N, Vonthein R, Knipper M, Engel J (2007) Thyroid hormone deficiency affects postnatal spiking activity and

- expression of Ca²⁺ and K⁺ channels in rodent inner hair cells. *J Neurosci* 27:3174-3186.
- Cartegni L, Chew SL, Krainer AR (2002) LISTENING TO SILENCE AND UNDERSTANDING NONSENSE: EXONIC MUTATIONS THAT AFFECT SPLICING. *Nature Reviews Genetics* Nat Rev Genet 3:285-298.
- Cartegni L, Wang J, Zhu Z, Zhang MQ, Krainer AR (2003) ESEfinder: A web resource to identify exonic splicing enhancers. *Nucleic Acids Res* 31:3568-3571.
- Conti E, Izaurralde E (2005) Nonsense-mediated mRNA decay: molecular insights and mechanistic variations across species. *Current Opinion in Cell Biology Nucleus and gene expression* 17:316-325.
- David Lenzi HvG (2001) Structure suggests function: the case for synaptic ribbons as exocytotic nanomachines. *BioEssays* 23:831-840.
- Edmonds BW, Gregory FD, Schweizer FE (2004) Evidence that fast exocytosis can be predominantly mediated by vesicles not docked at active zones in frog saccular hair cells. *J Physiol* 560:439-450.
- El-Amraoui A, Petit C (2005) Usher I syndrome: unravelling the mechanisms that underlie the cohesion of the growing hair bundle in inner ear sensory cells. *J Cell Sci* 118:4593-4603.
- Farris HE, LeBlanc CL, Goswami J, Ricci AJ (2004) Probing the pore of the auditory hair cell mechanotransducer channel in turtle. *J Physiol* 558:769-792.

- Fernandez-Alfonso T, Kwan R, Ryan TA (2006) Synaptic Vesicles Interchange Their Membrane Proteins with a Large Surface Reservoir during Recycling. *Neuron* 51:179-186.
- Freneau J, Robert T, Troyer MD, Pahner I, Nygaard GO, Tran CH, Reimer RJ, Bellocchio EE, Fortin D, Storm-Mathisen J, Edwards RH (2001) The Expression of Vesicular Glutamate Transporters Defines Two Classes of Excitatory Synapse. *Neuron* 31:247-260.
- Freneau RT, Jr., Voglmaier S, Seal RP, Edwards RH (2004a) VGLUTs define subsets of excitatory neurons and suggest novel roles for glutamate. *Trends Neurosci* 27:98-103.
- Freneau RT, Jr., Kam K, Qureshi T, Johnson J, Copenhagen DR, Storm-Mathisen J, Chaudhry FA, Nicoll RA, Edwards RH (2004b) Vesicular glutamate transporters 1 and 2 target to functionally distinct synaptic release sites. *Science* 304:1815-1819.
- Freneau RT, Jr., Burman J, Qureshi T, Tran CH, Proctor J, Johnson J, Zhang H, Sulzer D, Copenhagen DR, Storm-Mathisen J, Reimer RJ, Chaudhry FA, Edwards RH (2002) The identification of vesicular glutamate transporter 3 suggests novel modes of signaling by glutamate. *Proc Natl Acad Sci U S A* 99:14488-14493.
- Furness DN, Lawton DM (2003) Comparative distribution of glutamate transporters and receptors in relation to afferent innervation density in the mammalian cochlea. *J Neurosci* 23:11296-11304.

- Gale JE, Marcotti W, Kennedy HJ, Kros CJ, Richardson GP (2001) FM1-43 dye behaves as a permeant blocker of the hair-cell mechanotransducer channel. *J Neurosci* 21:7013-7025.
- Glowatzki E, Fuchs PA (2002) Transmitter release at the hair cell ribbon synapse. *Nat Neurosci* 5:147-154.
- Grant KA, Raible DW, Piotrowski T (2005) Regulation of latent sensory hair cell precursors by glia in the zebrafish lateral line. *Neuron* 45:69-80.
- Gras C, Herzog E, Bellenchi GC, Bernard V, Ravassard P, Pohl M, Gasnier B, Giros B, El Mestikawy S (2002) A third vesicular glutamate transporter expressed by cholinergic and serotonergic neurons. *J Neurosci* 22:5442-5451.
- Grati M, Schneider ME, Lipkow K, Strehler EE, Wenthold RJ, Kachar B (2006) Rapid turnover of stereocilia membrane proteins: evidence from the trafficking and mobility of plasma membrane Ca(2+)-ATPase 2. *J Neurosci* 26:6386-6395.
- Griesinger CB, Richards CD, Ashmore JF (2002) FM1-43 Reveals Membrane Recycling in Adult Inner Hair Cells of the Mammalian Cochlea
20026397. *J Neurosci* 22:3939-3952.
- Griesinger CB, Richards CD, Ashmore JF (2004) Apical endocytosis in outer hair cells of the mammalian cochlea
doi:10.1111/j.0953-816X.2004.03452.x. *European Journal of Neuroscience* 20:41-50.
- Griesinger CB, Richards CD, Ashmore JF (2005) Fast vesicle replenishment allows indefatigable signalling at the first auditory synapse. *J Neurosci* 25:212-215.
- Hayashi M, Otsuka M, Morimoto R, Hirota S, Yatsushiro S, Takeda J, Yamamoto A, Moriyama Y (2001) Differentiation-associated Na⁺-dependent inorganic

phosphate cotransporter (DNPI) is a vesicular glutamate transporter in endocrine glutamatergic systems. *J Biol Chem* 276:43400-43406.

Herzog E, Bellenchi GC, Gras C, Bernard V, Ravassard P, Bedet C, Gasnier B, Giros B, El Mestikawy S (2001a) The existence of a second vesicular glutamate transporter specifies subpopulations of glutamatergic neurons. *J Neurosci* 21:RC181.

Herzog E, Bellenchi GC, Gras C, Bernard V, Ravassard P, Bedet C, Gasnier B, Giros B, El Mestikawy S (2001b) The Existence of a Second Vesicular Glutamate Transporter Specifies Subpopulations of Glutamatergic Neurons. *J Neurosci* 21:181RC-.

Jung SK, Morimoto R, Otsuka M, Omote H (2006) Transmembrane topology of vesicular glutamate transporter 2. *Biol Pharm Bull* 29:547-549.

Khimich D, Nouvian R, Pujol R, Tom Dieck S, Egner A, Gundelfinger ED, Moser T (2005) Hair cell synaptic ribbons are essential for synchronous auditory signalling. *Nature* 434:889-894.

Kitajiri S, Fukumoto K, Hata M, Sasaki H, Katsuno T, Nakagawa T, Ito J, Tsukita S (2004) Radixin deficiency causes deafness associated with progressive degeneration of cochlear stereocilia. *J Cell Biol* 166:559-570.

Kremer H, van Wijk E, Marker T, Wolfrum U, Roepman R (2006) Usher syndrome: molecular links of pathogenesis, proteins and pathways. *Hum Mol Genet* 15 Spec No 2:R262-270.

Lenzi D, Crum J, Ellisman MH, Roberts WM (2002) Depolarization redistributes synaptic membrane and creates a gradient of vesicles on the synaptic body at a ribbon synapse. *Neuron* 36:649-659.

- Lenzi D, Runyeon JW, Crum J, Ellisman MH, Roberts WM (1999) Synaptic vesicle populations in saccular hair cells reconstructed by electron tomography. *J Neurosci* 19:119-132.
- Masino MA, Fetcho JR (2005) Fictive Swimming Motor Patterns in Wild Type and Mutant Larval Zebrafish
10.1152/jn.01248.2004. *J Neurophysiol* 93:3177-3188.
- Mathews DH, Sabina J, Zuker M, Turner DH (1999) Expanded sequence dependence of thermodynamic parameters improves prediction of RNA secondary structure. *J Mol Biol* 288:911-940.
- Matlin AJ, Clark F, Smith CWJ (2005) UNDERSTANDING ALTERNATIVE SPLICING: TOWARDS A CELLULAR CODE. *Nature Reviews Molecular Cell Biology*
Nat Rev Mol Cell Biol 6:386-398.
- McGee J, Goodyear RJ, McMillan DR, Stauffer EA, Holt JR, Locke KG, Birch DG, Legan PK, White PC, Walsh EJ, Richardson GP (2006) The Very Large G-Protein-Coupled Receptor VLGR1: A Component of the Ankle Link Complex Required for the Normal Development of Auditory Hair Bundles
10.1523/JNEUROSCI.0693-06.2006. *J Neurosci* 26:6543-6553.
- McLean DL, Fan J, Higashijima S-i, Hale ME, Fetcho JR (2007) A topographic map of recruitment in spinal cord. *J Neurosci* 27:446:71-75.
- Meyer J, Furness DN, Zenner HP, Hackney CM, Gummer AW (1998) Evidence for opening of hair-cell transducer channels after tip-link loss. *J Neurosci* 18:6748-6756.

- Meyers JR, MacDonald RB, Duggan A, Lenzi D, Standaert DG, Corwin JT, Corey DP (2003) Lighting up the senses: FM1-43 loading of sensory cells through nonselective ion channels. *J Neurosci* 23:4054-4065.
- Michel V, Goodyear RJ, Weil D, Marcotti W, Perfettini I, Wolfrum U, Kros CJ, Richardson GP, Petit C (2005) Cadherin 23 is a component of the transient lateral links in the developing hair bundles of cochlear sensory cells. *Dev Biol* 280:281-294.
- Moser T, Beutner D (2000) Kinetics of exocytosis and endocytosis at the cochlear inner hair cell afferent synapse of the mouse. *Proc Natl Acad Sci U S A* 97:883-888.
- Moser T, Brandt A, Lysakowski A (2006) Hair cell ribbon synapses. *Cell Tissue Res* 326:347-359.
- Muresan V, Lyass A, Crap BJ (1999) The Kinesin Motor KIF3A Is a Component of the Presynaptic Ribbon in Vertebrate Photoreceptors. *J Neurosci* 19:1027-1037.
- Ni B, Rosteck PR, Jr., Nadi NS, Paul SM (1994) Cloning and expression of a cDNA encoding a brain-specific Na(+)-dependent inorganic phosphate cotransporter. *Proc Natl Acad Sci U S A* 91:5607-5611.
- Nicolson T, Rusch A, Friedrich RW, Granato M, Ruppertsberg JP, Nusslein-Volhard C (1998) Genetic analysis of vertebrate sensory hair cell mechanosensation: the zebrafish circler mutants. *Neuron* 20:271-283.
- Pataký F, Pironkova R, Hudspeth AJ (2004) Radixin is a constituent of stereocilia in hair cells. *Proc Natl Acad Sci U S A* 101:2601-2606.
- Prescott ED, Zenisek D (2005) Recent progress towards understanding the synaptic ribbon. *Current Opinion in Neurobiology*

Sensory systems 15:431-436.

Preyer S, Hemmert W, Zenner HP, Gummer AW (1995) Abolition of the receptor potential response of isolated mammalian outer hair cells by hair-bundle treatment with elastase: a test of the tip-link hypothesis. *Hear Res* 89:187-193.

Roux I, Safieddine S, Nouvian R, Grati M, Simmler MC, Bahloul A, Perfettini I, Le Gall M, Rostaing P, Hamard G, Triller A, Avan P, Moser T, Petit C (2006) Otoferlin, defective in a human deafness form, is essential for exocytosis at the auditory ribbon synapse. *Cell* 127:277-289.

Rzadzinska A, Schneider M, Noben-Trauth K, Bartles JR, Kachar B (2005) Balanced levels of Espin are critical for stereociliary growth and length maintenance. *Cell Motil Cytoskeleton* 62:157-165.

Rzadzinska AK, Schneider ME, Davies C, Riordan GP, Kachar B (2004) An actin molecular treadmill and myosins maintain stereocilia functional architecture and self-renewal. *J Cell Biol* 164:887-897.

Safieddine S, Wenthold RJ (1999) SNARE complex at the ribbon synapses of cochlear hair cells: analysis of synaptic vesicle- and synaptic membrane-associated proteins. *Eur J Neurosci* 11:803-812.

Schafer MK, Varoqui H, Defamie N, Weihe E, Erickson JD (2002) Molecular cloning and functional identification of mouse vesicular glutamate transporter 3 and its expression in subsets of novel excitatory neurons. *J Biol Chem* 277:50734-50748.

Schmitz F, Königstorfer A, Südhof TC (2000) RIBEYE, a component of synaptic ribbons: a protein's journey through evolution provides insight into synaptic ribbon function. *Neuron* 28:857-872.

- Schnee ME, Lawton DM, Furness DN, Benke TA, Ricci AJ (2005) Auditory hair cell-afferent fiber synapses are specialized to operate at their best frequencies. *Neuron* 47:243-254.
- Schneider ME, Belyantseva IA, Azevedo RB, Kachar B (2002) Rapid renewal of auditory hair bundles. *Nature* 418:837-838.
- Schoch S, Gundelfinger E (2006) Molecular organization of the presynaptic active zone. *Cell and Tissue Research* 326:379-391.
- Seiler C, Finger-Baier KC, Rinner O, Makhankov YV, Schwarz H, Neuhauss SC, Nicolson T (2005) Duplicated genes with split functions: independent roles of protocadherin15 orthologues in zebrafish hearing and vision. *Development* 132:615-623.
- Sendin G, Bulankina AV, Riedel D, Moser T (2007) Maturation of ribbon synapses in hair cells is driven by thyroid hormone. *J Neurosci* 27:3163-3173.
- Sidi S, Busch-Nentwich E, Friedrich R, Schoenberger U, Nicolson T (2004) gemini encodes a zebrafish L-type calcium channel that localizes at sensory hair cell ribbon synapses. *J Neurosci* 24:4213-4223.
- Siemens J, Lillo C, Dumont RA, Reynolds A, Williams DS, Gillespie PG, Muller U (2004) Cadherin 23 is a component of the tip link in hair-cell stereocilia. *Nature* 428:950-955.
- Smear MC, Tao HW, Staub W, Orger MB, Gosse NJ, Liu Y, Takahashi K, Poo MM, Baier H (2007) Vesicular glutamate transport at a central synapse limits the acuity of visual perception in zebrafish. *Neuron* 53:65-77.

- Smith PJ, Zhang C, Wang J, Chew SL, Zhang MQ, Krainer AR (2006) An increased specificity score matrix for the prediction of SF2/ASF-specific exonic splicing enhancers. *Hum Mol Genet* 15:2490-2508.
- Sobkowicz HM, Rose JE, Scott GE, Slapnick SM (1982) Ribbon synapses in the developing intact and cultured organ of Corti in the mouse. *J Neurosci* 2:942-957.
- Sollner C, Rauch GJ, Siemens J, Geisler R, Schuster SC, Muller U, Nicolson T (2004) Mutations in cadherin 23 affect tip links in zebrafish sensory hair cells. *Nature* 428:955-959.
- Sudhof TC (2004) THE SYNAPTIC VESICLE CYCLE
doi:10.1146/annurev.neuro.26.041002.131412. *Annual Review of Neuroscience* 27:509-547.
- Takamori S, Rhee JS, Rosenmund C, Jahn R (2000) Identification of a vesicular glutamate transporter that defines a glutamatergic phenotype in neurons. *Nature* 407:189-194.
- Takamori S, Rhee JS, Rosenmund C, Jahn R (2001a) Identification of differentiation-associated brain-specific phosphate transporter as a second vesicular glutamate transporter (VGLUT2). *J Neurosci* 21:RC182.
- Takamori S, Rhee JS, Rosenmund C, Jahn R (2001b) Identification of Differentiation-Associated Brain-Specific Phosphate Transporter as a Second Vesicular Glutamate Transporter (VGLUT2). *J Neurosci* 21:182RC-.
- Takamori S, Malherbe P, Broger C, Jahn R (2002) Molecular cloning and functional characterization of human vesicular glutamate transporter 3. *EMBO Rep* 3:798-803.

- Tilney LG, Saunders JC (1983) Actin filaments, stereocilia, and hair cells of the bird cochlea. I. Length, number, width, and distribution of stereocilia of each hair cell are related to the position of the hair cell on the cochlea. *J Cell Biol* 96:807-821.
- Tilney LG, DeRosier DJ (1986) Actin filaments, stereocilia, and hair cells of the bird cochlea. IV. How the actin filaments become organized in developing stereocilia and in the cuticular plate. *Dev Biol* 116:119-129.
- Tilney LG, Egelman EH, DeRosier DJ, Saunderson JC (1983) Actin filaments, stereocilia, and hair cells of the bird cochlea. II. Packing of actin filaments in the stereocilia and in the cuticular plate and what happens to the organization when the stereocilia are bent. *J Cell Biol* 96:822-834.
- Varani L, Hasegawa M, Spillantini MG, Smith MJ, Murrell JR, Ghetti B, Klug A, Goedert M, Varani G (1999) Structure of tau exon 10 splicing regulatory element RNA and destabilization by mutations of frontotemporal dementia and parkinsonism linked to chromosome 17
10.1073/pnas.96.14.8229. *PNAS* 96:8229-8234.
- Vollrath MA, Kwan KY, Corey DP (2007) The Micromachinery of Mechanotransduction in Hair Cells
doi:10.1146/annurev.neuro.29.051605.112917. *Annual Review of Neuroscience* 30.
- Von Kriegstein K, Schmitz F, Link E, Sudhof TC (1999) Distribution of synaptic vesicle proteins in the mammalian retina identifies obligatory and facultative components of ribbon synapses. *Eur J Neurosci* 11:1335-1348.
- Wienisch M, Klingauf J (2006) Vesicular proteins exocytosed and subsequently retrieved by compensatory endocytosis are nonidentical. *J Biol Chem* 281:1019-1027.

Willig KI, Rizzoli SO, Westphal V, Jahn R, Hell SW (2006) STED microscopy reveals that synaptotagmin remains clustered after synaptic vesicle exocytosis. *440:935-939*.

Zhao Y, Yamoah EN, Gillespie PG (1996) Regeneration of broken tip links and restoration of mechanical transduction in hair cells. *Proc Natl Acad Sci U S A 93:15469-15474*.

Zheng L, Sekerkova G, Vranich K, Tilney LG, Mugnaini E, Bartles JR (2000) The deaf jerker mouse has a mutation in the gene encoding the espin actin-bundling proteins of hair cell stereocilia and lacks espins. *Cell 102:377-385*.

Zuker M (2003) Mfold web server for nucleic acid folding and hybridization prediction. *Nucleic Acids Res 31:3406-3415*.

APPENDIX 1: Interspecies Vglut3 Protein Alignment

d. rerio Vgl3.pro	HP_LGGFAGLKEKLNPGKEELKNMGDSLGLDQKIDVSNNEEDNIELTEEDGRPVAAAPKRSPPLDCCD	69
rat vglut3.pro	HPFKAFDTFKEKILKPGKEGKNAVGDLSGLLQKIDGTNEEDDAIELSEEGRPVQTSRARPVCCDCSC	69
mouse vglut3.pro	HPFKAFDTFKEKILKPGKEGKNAVGDLSGLLQKIDGTNEEDDAIELNEEGRPVQTSRARPVCCDCSC	69
human vglut3.pro	HPFKAFDTFKEKILKPGKEGKNAVGDLSGLLQKIDGTNEEDDAIELNEEGRPVQTSRARPVCCDCSC	69
d. rerio Vgl3.pro	FELPK-----RYIIAIIISGLGFCISFGIRCNLGVAVIEMVNNSTVYINGTAVHIDAGFNWDP	126
rat vglut3.pro	CGLPK-----RYIIAVMSLGLGFCISFGIRCNLGVAVIEMVNNSTVYVDDGKPEIQTAGFNWDP	126
mouse vglut3.pro	CGLPKRYICDCSCCGIPKRYIIAVMSLGLGFCISFGIRCNLGVAVIEMVNNSTVYVDDGKPEIQTAGFNWDP	139
human vglut3.pro	CGLPK-----RYIIAIIISGLGFCISFGIRCNLGVAVIEMVNNSTVYVDDGKPEIQTAGFNWDP	126
d. rerio Vgl3.pro	ETVGLIHGSFFWGYIVTQIPGGFISNKFANRVFGAAIFLTSVNNMIPSAARVHYGCVHVRILQGLVE	196
rat vglut3.pro	ETVGLIHGSFFWGYIVTQIPGGFISNKFANRVFGAAIFLTSVNNMIPSAARVHYGCVHVRILQGLVE	196
mouse vglut3.pro	ETVGLIHGSFFWGYIVTQIPGGFISNKFANRVFGAAIFLTSVNNMIPSAARVHYGCVHVRILQGLVE	209
human vglut3.pro	ETVGLIHGSFFWGYIVTQIPGGFISNKFANRVFGAAIFLTSVNNMIPSAARVHYGCVHVRILQGLVE	196
d. rerio Vgl3.pro	GVTYPACHGMVSKVAPPLERSRLATTSFCGSYAGAVVAMPLAGLVQYVIGWASVFYIYGHFGIIVYHFWL	266
rat vglut3.pro	GVTYPACHGMVSKVAPPLERSRLATTSFCGSYAGAVVAMPLAGLVQYVIGWASVFYIYGHFGIIVYHFWL	266
mouse vglut3.pro	GVTYPACHGMVSKVAPPLERSRLATTSFCGSYAGAVVAMPLAGLVQYVIGWASVFYIYGHFGIIVYHFWL	279
human vglut3.pro	GVTYPACHGMVSKVAPPLERSRLATTSFCGSYAGAVVAMPLAGLVQYVIGWASVFYIYGHFGIIVYHFWL	266
d. rerio Vgl3.pro	LAVNSPAVHPTISEERVIETSIIGEGANLISSTEFITPVRFFTSIPVYAIIVANFCRSWTFYLLLI	336
rat vglut3.pro	LQAYECPAAHPTISNEERTYIETSIIGEGANLASLTKFNTPVRRFFTSIPVYAIIVANFCRSWTFYLLLI	335
mouse vglut3.pro	LQAYECPAAHPTISNEERTYIETSIIGEGANLASLTKFNTPVRRFFTSIPVYAIIVANFCRSWTFYLLLI	348
human vglut3.pro	LQAYECPAAHPTISNEERTYIETSIIGEGANLASLTKFNTPVRRFFTSIPVYAIIVANFCRSWTFYLLLI	335
d. rerio Vgl3.pro	SQPAYFEEVFGFAISKVGLLSAVPHMNTIVVPIGGQLADYLRSRKILTTAVRKHNCGGFGHEATLLL	406
rat vglut3.pro	SQPAYFEEVFGFAISKVGLLSAVPHMNTIVVPIGGQLADYLRSRKILTTAVRKHNCGGFGHEATLLL	405
mouse vglut3.pro	SQPAYFEEVFGFAISKVGLLSAVPHMNTIVVPIGGQLADYLRSRKILTTAVRKHNCGGFGHEATLLL	418
human vglut3.pro	SQPAYFEEVFGFAISKVGLLSAVPHMNTIVVPIGGQLADYLRSRKILTTAVRKHNCGGFGHEATLLL	405
d. rerio Vgl3.pro	VWFSHTKGVAVISFLVAVGFSGFAISGFNWNHLDIAPRYASILNGISNGVGLTSGMVCPLIVGAMTKK	476
rat vglut3.pro	VWFSHTKGVAVISFLVAVGFSGFAISGFNWNHLDIAPRYASILNGISNGVGLTSGMVCPLIVGAMTKK	475
mouse vglut3.pro	VWFSHTKGVAVISFLVAVGFSGFAISGFNWNHLDIAPRYASILNGISNGVGLTSGMVCPLIVGAMTKK	488
human vglut3.pro	VWFSHTKGVAVISFLVAVGFSGFAISGFNWNHLDIAPRYASILNGISNGVGLTSGMVCPLIVGAMTKK	475
d. rerio Vgl3.pro	TRLEWQVFLIAALVHYSGVIFYGVFASGEKQWADPENISEEKCGIIDDELAEETELNHEFVSPRKK	546
rat vglut3.pro	TREEWQVFLIAALVHYSGVIFYGVFASGEKQWADPENISEEKCGIIDDELAEETELNHEFVSPRKK	545
mouse vglut3.pro	TREEWQVFLIAALVHYSGVIFYGVFASGEKQWADPENISEEKCGIIDDELAEETELNHEFVSPRKK	558
human vglut3.pro	TREEWQVFLIAALVHYSGVIFYGVFASGEKQWADPENISEEKCGIIDDELAEETELNHEFVSPRKK	545
d. rerio Vgl3.pro	TIRGTTDSSGRDGMKXKRGVTHQAEEDHESAHYENGEYQIDYQ	591
rat vglut3.pro	NSYGATTONCEVQKTRRQDRSAFDEEPLSYONEEIDFSETS	589
mouse vglut3.pro	NSYGATTONCEVQKTEWRQDRSAFDGEEPLSYQAEIDFSETS	681
human vglut3.pro	NSYGATTONCEVQKTEWRQDRSAFDGEEPLSYQAEIDFSETS	589

A CLUSTALW (MegAlign, DNASTar) alignment of Vglut3 across species. *D. rerio* Vglut3 shows ~78% sequence identity with its mammalian orthologues. The first and last TM domains are indicated with red bars, and the conserved dileucine-like motif is boxed.

APPENDIX 2: Alignment of *D. rerio* Vgluts.

mouse vglut1	-----MFRQK-----KRLA -----MEIKPD-----RFAQAKTQKIDOLLEKROQNGE-----TLLGAEHPELVEEKELP -----MDTVNRYVLADGKPKRGLAKTGGDQAVYKPKKTKGE-----VILLTEDGRPAQDNEKAPLADGCTC -----MFTPRP-----PAGFSYEGKMLANGLQAVYAVYKPKKPKGE-----NILLTEDGRPAQDNEKAPLADGCTC -----MEFTPRP-----PAGFSYEGKMLANGLQAVYAVYKPKKPKGE-----NILLTEDGRPAQDNEKAPLADGCTC d. rerio Vg3.pro	56 56 64 63 63 69
mouse vglut1	FGLPRRYIIAIDSGLGFCISFGIRCNLGVATVSMVNSGTVHRSKAVVIVAAQFSDNDFETVGLDNGSFFM FGLPRRYIIAIDSGLGFCISFGIRCNLGVATVSMVNSGTVYSGKXFPVIVAAQFSDNDFETVGLDNGSFFM FGLPRRYIIAIDSGLGFCISFGIRCNLGVATVSMVNSGTVHRSKAVVIVAAQFSDNDFETVGLDNGSFFM FGLPRRYIIAIDSGLGFCISFGIRCNLGVATVSMVNSGTVHRSKAVVIVAAQFSDNDFETVGLDNGSFFM FGLPRRYIIAIDSGLGFCISFGIRCNLGVATVSMVNSGTVHRSKAVVIVAAQFSDNDFETVGLDNGSFFM d. rerio Vg3.pro	125 125 134 133 114 138
mouse vglut1	SYIVTDIPGGFICQNFYAAANRVFGFAIVATSTLNMQIPSAARVHYGCVIVRILQGLVEGVYTPACMGHMS SYIVTDIPGGFICQNFYAAANRVFGFAIVATSTLNMQIPSAARVHYGCVIVRILQGLVEGVYTPACMGHMA SYIVTDIPGGFICSSRLAANRVFGAAILLTSTLNMQIPSAARVHYGCVIVRILQGLVEGVYTPACMGHMS SYIVTDIPGGFICSSRLAANRVFGAAILLTSTLNMQIPSAARVHYGCVIVRILQGLVEGVYTPACMGHMS SYIVTDIPGGFICSSRLAANRVFGAAILLTSTLNMQIPSAARVHYGCVIVRILQGLVEGVYTPACMGHMS d. rerio Vg3.pro	195 195 204 203 204 188
mouse vglut1	KWAPPLERSRLATTSFCGSYAGAVIANGLAGILVQYSGKGSVFFYVGGVFGIENYHILWLSYSPADNPT KWAPPLERSRLATTSFCGSYAGAVIANGLAGILVQYSGKGSVFFYVGGVFGIENYHILWLSYSPADNPT KWAPPLERSRLATTSFCGSYAGAVIANGLAGILVQYSGKGSVFFYVGGVFGIENYHILWLSYSPADNPT KWAPPLERSRLATTSFCGSYAGAVIANGLAGILVQYSGKGSVFFYVGGVFGIENYHILWLSYSPADNPT KWAPPLERSRLATTSFCGSYAGAVIANGLAGILVQYSGKGSVFFYVGGVFGIENYHILWLSYSPADNPT d. rerio Vg3.pro	265 265 274 273 254 278
mouse vglut1	ISIEERNYIEADIGESANLGNPLNPLNPTWRRFFTSMPVYALIVANFCRSWTFVLLLSIQPAFYEEVFGF ISIEERNYIEADIGESANLGNPLNPLNPTWRRFFTSMPVYALIVANFCRSWTFVLLLSIQPAFYEEVFGF ISIEERNYIEADIGESANLGNPLNPLNPTWRRFFTSMPVYALIVANFCRSWTFVLLLSIQPAFYEEVFGF ISIEERNYIEADIGESANLGNPLNPLNPTWRRFFTSMPVYALIVANFCRSWTFVLLLSIQPAFYEEVFGF ISIEERNYIEADIGESANLGNPLNPLNPTWRRFFTSMPVYALIVANFCRSWTFVLLLSIQPAFYEEVFGF d. rerio Vg3.pro	335 335 344 343 278 348
mouse vglut1	EISKVGWLSAAPHNVTIIVPISGQADFLRSRKHSTWVRLIDKCGGFGMEA TLLLVVGF SWSKQVAI EISKVGWLSAAPHNVTIIVPISGQADFLRSRKHSTWVRLIDKCGGFGMEA TLLLVVGF SWSKQVAI EISKVGWLSAAPHNVTIIVPISGQADFLRSRKHSTWVRLIDKCGGFGMEA TLLLVVGF SWSKQVAI EISKVGWLSAAPHNVTIIVPISGQADFLRSRKHSTWVRLIDKCGGFGMEA TLLLVVGF SWSKQVAI EISKVGWLSAAPHNVTIIVPISGQADFLRSRKHSTWVRLIDKCGGFGMEA TLLLVVGF SWSKQVAI d. rerio Vg3.pro	405 405 414 413 344 418
mouse vglut1	SFLNLAVGFSGFAISGFNVNHLDIAPRYASILMGISNGVGLSGHWCPILVGAITKTKTRSEWQVVFLLIA SFLNLAVGFSGFAISGFNVNHLDIAPRYASILMGISNGVGLSGHWCPILVGAITKTKTRSEWQVVFLLIA SFLNLAVGFSGFAISGFNVNHLDIAPRYASILMGISNGVGLSGHWCPILVGAITKTKTRSEWQVVFLLIA SFLNLAVGFSGFAISGFNVNHLDIAPRYASILMGISNGVGLSGHWCPILVGAITKTKTRSEWQVVFLLIA SFLNLAVGFSGFAISGFNVNHLDIAPRYASILMGISNGVGLSGHWCPILVGAITKTKTRSEWQVVFLLIA d. rerio Vg3.pro	475 475 484 483 414 488
mouse vglut1	SLVHYTSVIFYSIFA SGEKQWADPEI SDEKCGIIDEELANE TQDITLGAFFGAQSALGAP---ANTY ALVHYTSVIFYSIFA SGEKQWADPEI SDEKCGIIDEELANE TQDITLGAFFGAQSALGAP---ANTY SLVHYTSVIFYSIFA SGEKQWADPEI SDEKCGIIDEELANE TQDITLGAFFGAQSALGAP---ANTY SLVHYTSVIFYSIFA SGEKQWADPEI SDEKCGIIDEELANE TQDITLGAFFGAQSALGAP---ANTY SLVHYTSVIFYSIFA SGEKQWADPEI SDEKCGIIDEELANE TQDITLGAFFGAQSALGAP---ANTY d. rerio Vg3.pro	531 542 552 545 476 548
mouse vglut1	GGGAGAGAGAVSILNDITLQVYQVYGTN---SYLYGEGEREHT GGGAGAGAGAVSILNDITLQVYQVYGTN---SYLYGEGEREHT GGGAGAGAGAVSILNDITLQVYQVYGTN---SYLYGEGEREHT GGGAGAGAGAVSILNDITLQVYQVYGTN---SYLYGEGEREHT GGGAGAGAGAVSILNDITLQVYQVYGTN---SYLYGEGEREHT d. rerio Vg3.pro	560 582 588 585 516 591

CLUSTALW alignment of *D. rerio* Vglut1, -2a/b/c, and -3, with murine Vglut1 for comparison. Shaded residues indicate conservation in *D. rerio* Vglut3. Notice that most of the dissimilarity occurs in the cytoplasmic N- and C-termini, while the core of transporter is fairly conserved. . The first and last TM domains are indicated with red bars, and the conserved dileucine-like motif is boxed.